PLOS COMPLEX SYSTEMS

RESEARCH ARTICLE

Leveraging mathematical modeling framework to guide regimen strategy for phage therapy

Zhiyuan Yu[1], Tiffany Luong[2], Selenne Banuelos[3], Andrew Sue[2], Hwayeon Ryu[4], Rebecca Segal[5], Dwayne R. Roach[2‡*], Qimin Huang[6‡*]

1 Department of Bioinformatics, University of Michigan, Ann Arbor, Michigan, United States of America, **2** Department of Biology, San Diego State University, San Diego, California, United States of America, **3** Department of Mathematics, California State University Channel Islands, Camarillo, California, United States of America, **4** Department of Mathematics and Statistics, Elon University, Elon, North Carolina, United States of America, **5** Department of Mathematics and Applied Mathematics, Virginia Commonwealth University, Richmond, Virginia, United States of America, **6** Department of Mathematical & Computational Sciences, The College of Wooster, Wooster, Ohio, United States of America

‡ These authors are joint senior authors on this work.
* dwayne.roach@sdsu.edu (DRR); qhuang@wooster.edu (QH)

Citation: Yu Z, Luong T, Banuelos S, Sue A, Ryu H, Segal R, et al. (2024) Leveraging mathematical modeling framework to guide regimen strategy for phage therapy. PLOS Complex Syst 1(3): e0000015. https://doi.org/10.1371/journal.pcsy.0000015

Editor: Jaehee Kim, Cornell University, UNITED STATES OF AMERICA

Received: March 15, 2024

Accepted: September 2, 2024

Published: November 5, 2024

Data Availability Statement: Data and relevant code for this research work are stored in GitHub: [https://github.com/stanfish06/phage.git].

Funding: This work was supported by the National Science Foundation LEAPS-MPS Award [grant number DMS-2316631 to QH]. This work was supported by the National Institutes of Health (1R01AI177997-01A1 to DR). TL would like to thank the Rees-Stealy Research Foundation for their support. This work was supported by The American Institute of Mathematics through its

Abstract

Bacteriophage (phage) cocktail therapy has been relied upon more and more to treat antibiotic-resistant infections. Understanding of the complex kinetics between phages, target bacteria, and the emergence of phage resistance remain hurdles to successful clinical outcomes. Building upon previous mathematical concepts, we develop biologically-motivated nonlinear ordinary differential equation models to explore single, cocktail, and sequential phage treatment modalities. While the optimal pairwise phage treatment strategy was the double simultaneous administration of two highly potent and asymmetrically binding phage strains, it appears unable to prevent the evolution of resistance. This treatment regimen did have a greater lysis efficiency, promoted higher phage population sizes, reduced bacterial density the most, and suppressed the evolution of resistance the longest compared to all other treatments strategies tested. Conversely, the combination of phages with polar potencies allows the more efficiently replicating phages to monopolize susceptible host cells, thereby quickly negating the intended compounding effect of cocktails. Together, we demonstrate that a biologically-motivated modeling-based framework can be leveraged to quantify the effects of each phage's properties to more precisely predict treatment responses.

Author summary

Antimicrobials are one of the most significant medical advancements and are largely responsible for the reduction in morbidity and mortality associated with infectious diseases and routine medical procedures. However, the emergence and spread of antimicrobial resistance (AMR) has outpaced the development and approval of new antimicrobials,

Structured Quartet Research Ensembles program to SB, HR, RS, and QH. The funders had no role in study design, data collection and analysis, decision to publish, or preparation of the manuscript. The corresponding authors had full access to all of the data and the final responsibility to submit it for publication.

Competing interests: The authors have declared that no competing interests exist.

which has risen AMR as one of the leading global public health threats of the 21st century. Bacteriophages (phages for short) have long been considered a new class of antibacterials that can selectively target and kill AMR bacteria with great efficiency. However, optimizing the efficacy of phage therapy has been challenging due to the complex nature of employing a virus-based therapeutic. In this study, we synthesized *in vitro* and *in silico* models to determine optimal two-phage combination cocktails that lead to the eradication of the pathogen *Pseudomonas aeruginosa*. In addition, we uncover the pharmacokinetics and pharmacodynamics of phages in cocktails that may lead to treatment failure. Our findings could lead to a reduction in the risk of complications and failure of phage candidates and speed up the development of more effective phage therapies against AMR disease.

1 Introduction

Phage therapy is a century-old infection remedy that has once again become a broadly relevant technology as an alternative or adjuvant to antibiotics to combat the rise of antibiotic resistance [1,2]. Phages, or formally bacteriophages, are a type of virus that specifically infect and kill bacteria. They can infect a bacterium by a range of biochemically diverse cell surface receptors and hijack the bacterium's cellular machinery to force the production of new phage particles [3]. Before long, the hijacked cell lyses to release the phage progeny. Phages are so successful at infecting bacteria that they are estimated to outnumber all bacteria on the planet by an order of magnitude [4,5]. However, phased clinical trials have not shown phage therapy to be more effective than existing antimicrobial treatments [1,2,6]. On the other hand, there is a growing catalog of successful single patient case studies or case series conducted as compassionate treatments [1,7–9]. Although the primary objective of compassionate treatment is to provide life-saving treatment to an individual patient rather than to conduct a controlled evaluation of the therapeutic agent, overall, these case reports reinforce and provide positive support for further phage therapy development.

By all accounts, phages are the most merciless killer of bacteria and present themselves as attractive candidates for antimicrobial therapy. Their other attributes include that they are self-replicative *in situ* (i.e. auto-dosing) that serves to prolong their half-life in the body, most have low toxicity, and antibiotic cross-resistance is rare [1,10–12]. However, evolutionary analyses of phage–bacteria dynamics suggests that predator and prey often co-evolve ways to avoid complete eradication of either phage or host bacteria [13]. This is accomplished in part through a tight coordination between bacterial population densities and phage resistance [14–17]. Therefore, efforts made to use phages as antimicrobials should determine the appropriate dose and regimen that alter the equilibrium between host and predator populations, moving this equilibrium towards host eradication.

More precise technologies are required to advance system-based approaches for studying bacterial response to phage therapy. We posit that a mechanistic, mathematical modeling framework is essential to maximize the knowledge gained through treatment response studies [18–23]. In this paradigm, biologically-motived mathematical models are constructed to describe observed behaviors of the preclinical system under investigation. The model is then fitted to experimental data, yielding a set of parameter values that provide mechanistic insight into observed data [18,23–27]. *In vitro*, compartmental models have been used to describe the temporal relationship between phages and target host bacteria [28–30]. For example, Payne and Jansen drew on the principles of population dynamics to model the density-dependent

qualities of phage replication [31]. The mathematical model allowed broad categorization of phage behavior to predict therapeutic outcomes based on phage density and bacterial growth. Pharmacokinetic (PK) (i.e. phage concentrations over time) and pharmacodynamics (PD) (i.e. phage effects over time) models have also been developed to investigate phage treatment response *in vivo* [18,23–27]. There are, however, challenges when developing models that reconstruct biologically observed behaviors of the system under investigation. For instance, previous mathematical models have yet to behave consistently across a wide spectrum of phage and treatment protocols, thereby being unable to demonstrate that the response dynamics of target host species is predictable within a mathematical framework. Moreover, Roach and colleagues found that non-biologically motivated mathematical models of phage therapy can oversimplify assumptions that are inconsistent with experimental observations [18]. That is, it is often assumed that phage lysis rates of bacteria are linear to viral density. Rarely factored is the spatial heterogeneity and viral saturation at the site of infection that can impede phage-bacteria interactions and thereby reduce phage lysis rate [18,19,32,33]. Although phage lysis is conceptually simple, the idea of finding the right treatment at the right dose for the right patient to ensure an appropriate balance of risks and benefits is challenging and requires a multidisciplinary approach.

Mathematical modeling approaches have played a central role in understanding and quantifying mechanisms in different antimicrobials. In this approach, biology-based hypotheses are expressed via mathematical relations and then tested based on empirical data. It is the goal of the present effort to demonstrate the utility of a mechanistic, mathematical modeling framework in quantifying treatment responses to strictly lytic phages administered individually or in combination. We leverage mathematical models to explore experimental data to yield quantitative measures of specific bacterial and viral processes for applying growth control regimens. First, we create an appropriate model of the dynamics of pathogen growth and the effects of phage treatment on the dynamics. The time-kill kinetics model is a quantitative technique to incorporate the effects of the particular phage strains of interest, namely LUZ19, E215 and PYO2. These individual phages are well characterized to rapidly and efficiently kill *P. aeruginosa* [34–38]. This bacterium is a notable nosocomial opportunistic pathogen that can cause severe infections in humans and animals. The emergence of multidrug resistant (MDR) *P. aeruginosa* has motivated the development of phage therapy to control infections [1,39,40]. The high-throughput format of time-kill kinetics allows for maximizing benefits of treatment while minimizing its side effects (e.g. selection of phage resistance). Next, we combined terms representing phage and bacteria effects, using appropriate signs and weights, to obtain a biologically-motivated ordinary differential equation (ODE). This allowed for the determination of parameter values to use for the system and to then use the model to explore parameter space representing other phage characteristics. We further exercised the model by proposing alternative bacteria growth control solution with a sequential regimen. As this approach accounts for variable properties of phages, we posit that it allows for more precise comparisons among target bacterial strains relative to *in vitro* based on optical density concentration. The modeling-based framework proposed in this work was leveraged to quantify the effects of various phage properties more precisely on treatment response.

The mathematical modeling for bacteriophage could be traced back to 1960 when Allan Campbell started to study how bacteria and bacteriophage coexist in nature[41]. Levin et al. [42] then later developed a delayed differential equation model to describe a predator-prey relationship between phages and bacteria under the influence of resource availability. Payne and Jansen developed mathematical models to describe phage-bacteria dynamics as being density-dependent [31,43]. The formulae included replication coefficient of the bacteria, the transmission coefficient, the lysis rate, the burst size, and the decay rate of free phages to analyze the

phage treatment failure thresholds. Cairns et al. developed a system of delay differential equations to account for the presence of phage susceptible and phage resistant cells which leads to delayed phage burst [28]. In 2005, Weitz et al. developed an ordinary differential model and a stochastic computational simulator to describe and investigate the interactions between different bacterial and phage strains as well as their adaptive phenotypic variations [44]. More recently, Bull et al. [45] developed an ODE model with separate variables for free bacteria and bacteria with low phage absorption rates to accommodate non-genetic heterogeneity in the population (e.g., biofilm). For the first time, mathematical models were extended to incorporate the kinetics between two host strains and two phage strains. The aforementioned model parameterized *in vitro* data in order to focus on pre-existing phage sensitive and insensitive subpopulations, but most features of phage infection and replication were absent [45]. Unlike previous studies that mainly focused on the phage killing aspect of phage therapy [30,46,47], our double phage models incorporate not only phage killing, but the evolution of and competition between bacterial phage resistant variants. We used this simplified approach for a well-mixed experimental environment because we aimed reveal the more subtle details of the bacteria and phage interactions, which. allowed us to elucidate general conclusions about the important phage characteristics.

2 Materials and Methods

A variety of microbiological assays exist to test phage infection and bacterial responses to infection ranging from plaque formation assays to dynamic microfluidic devices. Our experiments use microplate time-kill assays, a gold standard to study the activity of antimicrobial agents *in vitro*, to demonstrate phage lytic and replicative properties and evolution of host bacteria to phage infection. The method uses a high-throughput 96 microwell format to measure bacterial growth under different phage exposures and conditions. In this work, we explore phage infection dynamics for the Gram-negative *P. aeruginosa* strain PAO1. We first performed a series of time-kill assays using 3 virulent (i.e. strictly lytic) phage strains, LUZ19, PYO2, and E215, which rapidly and efficiently lyse strain PAO1 *in vitro*. Characterization of single phage treatments as well as double phage cocktail treatments were compared to demonstrate phage-bacteria outcomes under the different treatment regimes. Using changes in bacterial density (measured by optical density (OD_{600})) we observed trends in bacterial killing and bacterial regrowth in the form of evolved phage resistance against one or more phage strains.

Next, we used the time-kill kinetics results and other known phage replication properties to develop and parameterize a mathematical framework for investigating the complexities of phage-bacteria interactions that were not resolved during *in vitro* experimentation. Based on *in vitro* data in Fig 1A–1C, we were able to estimate key parameters in our mathematical models and draw general conclusions about the important phage characteristics.

Experiment design and data description

Strains, media, and growth conditions. *P. aeruginosa* laboratory strain PAO1 was grown aerobically in Luria-Bertani (LB) broth Lennox (10g tryptone, 5g NaCl, 5g yeast extract per L) at 37˚C with shaking. LB supplemented with 1.5% agar allowed for solid medium growth when required. Stock vials were preserved at −80˚C in LB broth with 25% glycerol and were streaked onto LB agar for each assay. The virulent tailed phage strain LUZ19 is a podovirus in the genus *Phikmvvirus* isolated on and capable of infecting PAO1 [48–50]. The virulent tailed phage strain PYO2 is a myovirus in the genus *Litunavirus* and the virulent tailed phage strain E215 is a myovirus in the genus *Pbunavirus*, were also isolated with PAO1 [34,51]. Phages were propagated and purified as previously described [52]. Briefly, phage and PAO1 cells were

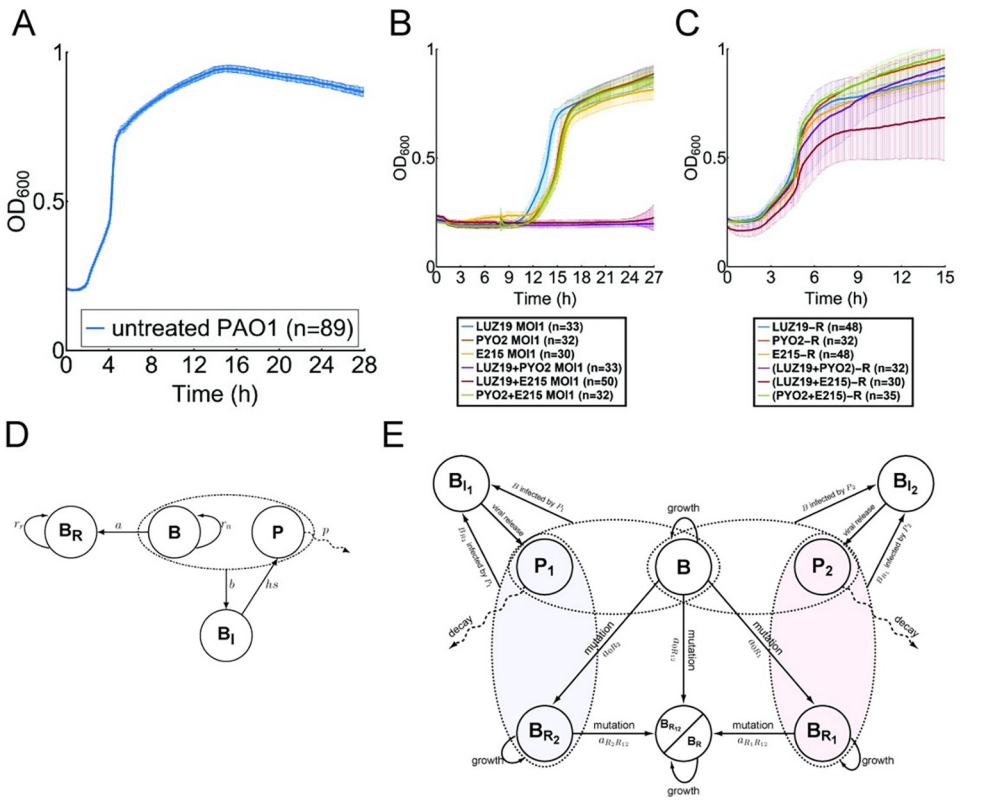

Fig 1. ***In vitro*** **data and schematic of each ODE model.** ***(A) P. aeruginosa PAO1 growth without the addition of phage. (B) P. aeruginosa PAO1 growth after single phage treatment with either phage LUZ19, PYO2, or E215, and after simultaneous double-phage cocktail treatment with a pair of phages from LUZ19, PYO2, and E215. (C) P. aeruginosa PAO1 bacteriophage insensitive mutants (BIM) growth. (D)*** *Schematic of a single phage interaction model. Bacteria (B) replicate at the rate (r_n). In the presence of phages (P) that decay at rate (p), sensitive bacteria either mutate (a) into phage resistant single-mutant bacteria (B_R) or are bound to and infected by phage (b). Infected bacteria are subsequently moved to the infected class (B_I). New phages are released when the infected bacteria cell is lysed (hs).* ***(E)*** *Schematic of a two-phage interaction model with and without collateral phage resistance. In the presence of phages (P_1 and P_2), bacteria (B) mutate to either receptor-specific single-mutant bacteria (B_{R_1}, B_{R_2}) which a phage using an alternate receptor (P_n) can still adsorb to, or become double-mutant bacteria ($B_{R_{12}}$) resistant to both receptors. Adsorbed bacteria are subsequently moved to the infected class, (B_{I_i})). If the two phages use the same receptor, collateral resistance occurs and the double-mutant is no different than the single mutant, that is $B_R = B_{R12}$ and no additional mutational outcomes emerge and B_{R1} and B_{R2} are omitted.*

https://doi.org/10.1371/journal.pcsy.0000015.g001

mixed at a multiplicity of infection (MOI) of 0.1 and incubated at 37˚C with shaking. Lysates were centrifuged twice at 8000×g and the supernatant 0.22 μm filter sterilized before being stored at 4˚C.

Spot$^+$ titration. Bacterial cultures and phage stocks were quantified by double aliquot 48-spot serial titration. Briefly, bacteria culture lawned over agar was air-dried. In a 96-well microplate, two identical stock samples were taken and each serially diluted at least 8 times before spotting 4 μL in triplicate on the dried bacterial lawn. Titrations were incubated at 37˚C until colony forming units (CFU) or plaque forming units (PFU) were visible.

Time-kill assay. The *Pseudomonas* inoculum was prepared freshly for each experiment by growing 30 μL from a 24 h CFU overnight culture in fresh LB broth under shaking conditions (120 rpm) to obtain cells in the early logarithmic phase of growth. Bacterial culture was diluted in fresh LB broth to inoculate each microplate well with 2×10^6 CFU and 2×10^6 PFU of test phage strain dispersed into flat bottom 96-well microtiter plates (Falcon) to obtain a MOI of 1.

Microtiter plates were sealed with BreathEasy^{TM} membrane (Diversified Biotech) and time-kill curves measured optical density (OD_{600nm}) at intervals of 6 min by a CLARIOstar reader (BMG Labtech). A growth control of *Pseudomonas* inoculum without phages and medium only sterility control were included for each experiment. Because the limit of detection (LOD) of the plate reader was OD_{600nm} 0.18 corresponding to 7.84×10^5 CFU/mL, bacterial titers below the limit of detection were determined on growth agar.

Evolution of resistance and fitness cost. Live bacterial cells remaining in time-kill microplate individual wells were streaked onto LB agar and grown at 37˚C for 24 h. Phage sensitivity was determined on pure cultures of each isolated colony and compared to an untreated PAO1 culture. Isolated bacteriophage insensitive mutants (BIMs) were stored in 25% glycerol at -80˚C. To determine the fitness cost that the phage resistance mechanism imposes on the bacterial cell, BIMs were revived from cold storage, streaked, and cultured overnight. A single CFU was grown in fresh LB broth to a density to inoculate each microplate well with 2×10^6 CFU and bacterial growth curves measured at intervals of 6 min by a CLARIOstar reader. A medium only sterility control was included, and all growth curves were repeated thrice.

Phage adsorption rates and one step growth. The rate at which an individual phage particle binds to the host cell surface was measured by decrease in free-phages in culture with sensitive cells [53]. Approximately, 1×10^7 PFU of phages were diluted in 9 mL of warm LB broth inoculated with $4.5x10^8$ CFU of PAO1 and incubated at 37˚C with shaking (120 rpm). Samples were taken at 1 min intervals, treated with chloroform, and centrifuged at 12,000×g for 3 min. Each timepoint was phage titrated using the Spot+ method. The one-step phage growth curve was measured as previously described [54]. Approximately 5×10^7 PFU of phages were diluted in 9 mL of warm LB broth inoculated with $4.95x10^8$ CFU of PAO1 and incubated at 37˚C with shaking (120 rpm). Two samples were taken at 2 min intervals, treated with and without chloroform, and centrifuged at 12,000×g for 3 min. Phages from each timepoint were titrated using the Spot+ method. Phage adsorption assays and one-step growth curves were each performed with three isolated CFUs.

DNA extraction, whole genome sequencing, and mutation calling. Bacterial colony DNA was isolated using the NucleoSpin^{TM} Microbial DNA Kit (Macherey-Nagel) as per the manufacturer's instructions. Purified DNA was eluted into water and submitted to SeqCenter (Pittsburgh, USA) for analysis. Whole genome sequencing (WGS) libraries were prepared by SeqCenter (Pittsburg, USA) using the Nextera DNA Library Preparation Kit (Illumina, USA) and libraries were sequenced using the NextSeq 550 system (Illumina, USA) with read length of 2× 150 bp. We trimmed and removed low quality raw reads using fastp v.0.20.1 [55] and genomes were both *de novo* assembled with SPAdes v.3.15.1 [56] and reference guided with MeDuSa v1.6 [57]. Genome annotation was generated using Rapid Annotations of Subsystems Technology (RAST) v2.0 [58] and breseq v.0.35.5 [59] assisted with identifying mutational patterns in BIMs. Default settings were used for all software.

Mathematical models

We organized the *in vitro* data based on the treatment regime in Fig 1A–1C. Each dataset allows us to estimate key parameters in our mathematical models (See S1 Fig, for details).

D1.Control: *P. aeruginosa* PAO1 growth without the addition of phage.

D2.Total bacterial density from single phage treatment: *P. aeruginosa* PAO1 growth after single phage treatment with either phage LUZ19, PYO2, or E215.

D3.Resistant bacteria strain from single phage treatment: *P. aeruginosa* PAO1 BIM growth.

D4.Total bacterial density from simultaneous double phage cocktail treatment: *P. aeruginosa* PAO1 growth after simultaneous double-phage cocktail treatment with a pair of phages from LUZ19, PYO2, and E215.

D5.Resistant bacteria strain from simultaneous double-phage treatment: *P. aeruginosa* PAO1 BIM growth.

Mathematical model of a single-phage and host interaction. The infection process begins with a phage particle attaching to the surface of the host bacterium via a specific cell surface receptor, which triggers the injection of the viral chromosome into the host cell cytoplasm. The localization, volume, and density of cell surface receptors play a pivotal role in the phage infection process and proteins that act as receptors may carry out a variety of functions for the bacterium [60]. Once in the cell, viral genetic material is translated to redirect cellular machinery to produce new phage particles and to lyse the cell to release them. Foundational work by Campbell [41], Levin et al. [42], Payne & Jansen [31,43], Cairns et al. [28], and more recently Bull et al. [45] were used to parameterize phage characteristics into equations and formulae that could more consistently predict and therefore model phage behavior under different scenarios. In particular, the application of ODE models to phage growth in the last several decades has enabled the modeling of both phages and their bacterial hosts with consideration of spatial effects in biology [61] or the emergence of bacterial resistance to phages [28]. Building upon these previous mathematical concepts, we developed a nonlinear four-compartment ODE model to explore phage-bacteria interactions most important to a single phage treatment (i.e., monophage therapy) of a target bacterial population. Fig 1D describes the density-dependent interactions between a single phage that targets phage-sensitive bacteria (B), free phage particles (P), phage infected bacteria (B_I), and evolved single-phage resistant bacteria (B_R). This interaction scenario with a single phage strain modelled through the system of Eq (1):

$$\begin{aligned}
\frac{dB}{dt} &= r_n B\left(1 - \frac{B + B_R}{K}\right) - aB - bBP \\
\frac{dB_I}{dt} &= bBP - sB_I \\
\frac{dB_R}{dt} &= r_r B_R\left(1 - \frac{B + B_R}{K}\right) + aB \\
\frac{dP}{dt} &= hsB_I - pP - bBP
\end{aligned} \tag{1}$$

Phage sensitive bacteria (B) were modeled to exhibit a logistic growth rate in the absence of phage infection, r_n, a carrying capacity K, and density dependence B+B_R (see Table 1 for a full list of definitions for the single phage model). We assume that B can evolve resistance spontaneously (B_R) with a mutation rate of a. The phage resistant single-mutant bacteria, B_R, grows logistically with growth rate r_r with no density loss due to phage infection or mutation. Phage dynamics have traditionally been modeled under the assumptions of mass action [62]. Using mass action as the foundation, we set the rate of phage adsorption (b) and assume that infected cells are only lysed by phages at a rate of s. Free phage growth results from the lysis of infected cells, B_I, with a virion burst size of h. We posit that phage decay rate, p, would be negligible in our closed *in vitro* model [63]. However, we assume that host stressors (e.g. immune system) can lead to the damage and decay of phages during treatment, and thus p was kept for future expansion. Payne and Jansen suggest that there are proliferation thresholds before phage density can increase [31]. Therefore, we assume that the reproduction number and the number of

Table 1. Phage and bacteria parameters used in the ODE models.

Symbol	Description	Value and 95% Confidence Interval	Reference
r_n	Basal growth rate of phage sensitive bacteria	0.880 [0.875; 0.885] h^{-1}	Calibrated
r_{r_a}	Basal growth rate of phage LUZ19-resistant bacteria	0.716 [0.709; 0.723] h^{-1}	Calibrated
r_{r_b}	Basal growth rate of phage PYO2-resistant bacteria	0.731 [0.718; 0.744] h^{-1}	Calibrated
r_{r_c}	Basal growth rate of phage E215-resistant bacteria	0.752 [0.744; 0.760] h^{-1}	Calibrated
b	Binding rate of phage to bacteria	382 [215; 598] $OD_{600}nm^{-1}h^{-1}$	Calibrated
h_a	Burst size at lysis for LUZ19	100	[50]
h_b	Burst size at lysis for PYO2	100	(This study)
h_c	Burst size at lysis for E215	200	(This study)
s_a	Lysis rate of bacteria infected by phage LUZ19	0.147 [0.123; 0.174] h^{-1}	Calibrated
s_b	Lysis rate of bacteria infected by phage PYO2	0.178 [0.137; 0.210] h^{-1}	Calibrated
s_c	Lysis rate of bacteria infected by phage E215	0.051 [0.044; 0.057] h^{-1}	Calibrated
a_p	Rate of generating pili-binding phage resistance	0.025 [0.019; 0.033] h^{-1}	Calibrated
a_l	Rate of generating LPS-binding phage resistance	0.012 [0.009; 0.015] h^{-1}	Calibrated
p	Background decay rate of phage	0.09 h^{-1}	[63]
K	Carrying capacity of bacteria	$(.)OD_{600nm}$	Varied

https://doi.org/10.1371/journal.pcsy.0000015.t001

secondary infections arising from a single infected cell, must be greater than 1 for phage infection to be productive. That is, each infected cell's lifespan is given by $1/s$ and produces $hs/s = h$ phage particles. In turn, each phage particle will cause $bB/(bB+p)$ new infections. Thus, we need $hbB/(bB+p)>1$. This implies that the initial density of bacteria must be above the proliferation threshold in order for the phages to replicate effectively, which is modeled as:

$$B = \frac{p}{b(h-1)} \tag{2}$$

The inundation threshold is the concentration of phage necessary to reduce the density of phage sensitive bacteria. Thus, we need $dB/dt<0$ and estimate $dB/dt = r_nB—bBP < 0$ to obtain the inundation threshold as:

$$P = \frac{r_n}{b} \tag{3}$$

Mathematical model of a two-phage combination treatment without collateral resistance. Next, we extended our single-phage model to describe interactions of two different phage strains simultaneously treated in combination (for model schematic see Fig 1E). Combining phage types in so called 'cocktails' can enhance the diversity of bacterial strains targeted and prevent the evolution of phage resistance [14,34,64,65]. In the single-phage model, only one single-mutant B_R outcome is expected when resistance emerges in response to phage infection. Our second model assumes that when two phage strains are added, that each phage type binds to different cell surface receptors and thus phage resistance can occur either stepwise to each phage strain wherein two types of phage-specific single-mutants are induced (B_1, B_2) or resistance to both phages occurs in a single cell (B_{12}). Because these mutational outcomes are phage-specific, this double-phage model therefore assumes that the two phages do not confer collateral resistance where $B_1 = / = B_2$. This lowers the probability of early phage resistance outgrowth since two different mutations within a single cell genome are required to evolve resistance [66]. For example, in our experimental data, PYO2, E215 and LUZ19 use the cell surface receptor of lipopolysaccharide (LPS), LPS, and pili, respectively. All the phages in a

cocktail of PYO2 and E215 will bind to the same cell surface receptor and select for 'collateral resistance' in isolated bacteriophage insensitive mutants (BIMs). Conversely, a combination of PYO2 and LUZ19, or E215 and LUZ19 will select for BIMs with independent gene mutations. This will cause the bacterial population to contain three subpopulations with (i) resistance to Phage 1, (ii) resistance to Phage 2, and (iii) resistance to both phage strains. This 2-phage combination treatment without collateral resistance is modeled through the system of Eqs (4):

$$\begin{aligned}
\frac{dB}{dt} &= r_n B(1-\frac{B_T}{K}) - a_{0R_1}B - a_{0R_2}B - a_{0R_{12}}B - bBP_1 - bBP_2\\
\frac{dB_{I_1}}{dt} &= bBP_1 + bB_{R_2}P_1 - s_1 B_{I_1}\\
\frac{dB_{I_2}}{dt} &= bBP_2 + bB_{R_1}P_2 - s_2 B_{I_2}\\
\frac{dB_{R_1}}{dt} &= r_1 B_{R_1}(1-\frac{B_T}{K}) + a_{0R_1}B - a_{R_1R_{12}}B_{R_1} - bB_{R_1}P_2\\
\frac{dB_{R_2}}{dt} &= r_2 B_{R_2}(1-\frac{B_T}{K}) + a_{0R_2}B - a_{R_2R_{12}}B_{R2} - bB_{R_2}P_1\\
\frac{dB_{R_{12}}}{dt} &= r_{12} B_{R_{12}}(1-\frac{B_T}{K}) + a_{0R_{12}}B + a_{R_1R_{12}}B_{R_1} + a_{R_2R_{12}}B_{R_2}\\
\frac{dP_1}{dt} &= hs_1 B_{I_1} - pP_1 - bBP_1 - bB_{R_2}P_1\\
\frac{dP_2}{dt} &= hs_2 B_{I_2} - pP_2 - bBP_2 - bB_{R_1}P_2
\end{aligned} \tag{4}$$

These equations include the density-dependent interactions between sensitive bacteria (B), strain 1 free phages (P_1), strain 2 free phages (P_2), phage strain 1 infected cells (B_{I_1}), phage strain 2 infected cells (B_{I_2}), evolved phage strain 1 resistant mutants (B_{R_1}), evolved phage strain 2 resistant mutants (B_{R_2}), and evolved bacterial resistance to both phage strains ($B_{R_{12}}$) (see Table 2 for a full list of definitions for the double-phage model). In the absence of phages, B, phage strain j- resistant bacteria (j = 1,2), and $B_{R_{12}}$ grow logistically with density dependence ($B_T = B + B_{R_1} + B_{R_2} + B_{R_{12}}$), carrying capacity K, and growth rate r_n, r_j, and $r12$, respectively. In contrast, in the presence of phage: i) B are either infected by phage strain P_j, at rate b, and lysed at a rate of s_j, or ii) B acquire resistance to one of the phage strains at rate a_{0R_j}, or acquire two mutations to gain simultaneous resistance to both phage strains at rate $a_{0R_{12}}$. Because the model is parameterized where each phage strain binds to a different receptor, if $a_{0R_1} := a_p$ then $a_{0R_2} := a_l$. Double mutant is denoted by $a_{0R_{12}} := a_{lp}$.

Phage strain j-resistant single-mutant bacteria, B_{R_j}, are infected by phage strain P_i $(i \neq j)$, at rate b. In contrast, $B_{R_{12}}$, cannot be infected by either phage strain. Phage strain j-resistant single-mutant bacteria mutate to double-mutant bacteria at rate $a_{R_jR_{12}}$. Given our possible scenarios, if $a_{0R_1} := a_l$, then $a_{R_1R_2} := a_p$, for example. Bacteria bound by phage strain P_j move to the B_{I_j} class.

Mathematical model of two-phages with collateral phage resistance. Two phages sharing the same binding receptor can elicit the same genotypic mutation during bacterial treatment where $B_{R_1} = B_{R_2}$. Because a single resistance mutation can confer resistance to multiple phages in solution, we re-parameterized the two-phage model to include collateral resistance whereby a single gene mutation can prevent either phage from infecting, B_R. For model

Table 2. Phage and bacteria parameters new to the two-phage treatment models.

Symbol	Description	Value and 95% Confidence Interval	Reference
a_{lp}	Rate of generating both pili-binding phage resistance and LPS-binding phage resistance simultaneously	$1.12 \times 10^{-5}[0, 5.69 \times 10^{-5}]h^{-1}$	Calibrated
r_{a+b}	Basal growth rate of bacteria with resistance to both phage LUZ19 and PYO2 in simultaneous simulation	0.607 [0.583; 0.631] h^{-1}	Calibrated
r_{a+c}	Basal growth rate of bacteria with resistance to both phage LUZ19 and E215 in simultaneous simulation	0.618 [0.590; 0.647] h^{-1}	Calibrated
r_{b+c}	Basal growth rate of bacteria with resistance to both phage PYO2 and E215 in simultaneous simulation	0.745 [0.733; 0.758] h^{-1}	Assumed equal to r_{r_b} in Table 1
$r_{a\to b}$	Basal growth rate of bacteria with resistance to both phage LUZ19 and PYO2 in phage (LUZ19→PYO2)-sequential simulation	0.546 [0.524; 0.568] h^{-1}	[14]
$r_{b\to a}$	Basal growth rate of bacteria with resistance to both phage PYO2 and LUZ19 in phage (PYO2→LUZ19)-sequential simulation	0.607 [0.583; 0.631] h^{-1}	[14]
$r_{a\to c}$	Basal growth rate of bacteria with resistance to both phage LUZ19 and E215 in phage (LUZ19→E215)-sequential simulation	0.556 [0.531; 0.582] h^{-1}	[14]
$r_{c\to a}$	Basal growth rate of bacteria with resistance to both phage E215 and LUZ19 in phage (E215→LUZ19)-sequential simulation	0.618 [0.590; 0.647] h^{-1}	[14]
$r_{b\to c}$	Basal growth rate of bacteria with resistance to both phage PYO2 and E215 in phage (PYO2→E215) -sequential simulation	0.731 [0.718; 0.744] h^{-1}	Assumed equal to r_{r_b} in Table 1
$r_{c\to b}$	Basal growth rate of bacteria with resistance to both phage E215 and PYO2 in phage (E215→PYO2)-sequential simulation	0.731 [0.718; 0.744] h^{-1}	Assumed equal to r_{r_b} in Table 1

https://doi.org/10.1371/journal.pcsy.0000015.t002

schematic see Fig 1E. The process for double-phage combinations with collateral resistance is modeled through system of Eq (5):

$$\begin{aligned}
\frac{dB}{dt} &= r_n B(1 - \frac{B + B_R}{K}) - aB - bBP_1 - bBP_2 \\
\frac{dB_{I_1}}{dt} &= bBP_1 - s_1 B_{I_1} \\
\frac{dB_{I_2}}{dt} &= bBP_2 - s_2 B_{I_2} \\
\frac{dB_R}{dt} &= r_r B_R(1 - \frac{B + B_R}{K}) + aB \\
\frac{dP_1}{dt} &= hs_1 B_{I_1} - pP_1 - bBP_1 \\
\frac{dP_2}{dt} &= hs_2 B_{I_2} - pP_2 - bBP_2
\end{aligned} \tag{5}$$

The system of Eq (5) for a two-phage collateral phage resistance model is similar to eq system (4) by omitting bacteria mutant outcomes B_{R_1} and B_{R_2}.

3 Results

Time–kill of single and cocktail formulations

Following the killing and growth of PAO1 as a function of time and phage concentrations showed that LUZ19 and PYO2 at MOI 1 reduced bacterial counts below the optical density (OD) limit of detection (LOD) for 10 and 12 hours, respectively (Fig 2A). We were able to determine that the OD_{600} LOD translated to $5.49{\times}10^4$ CFU per microwell from bacterial counts at time zero on growth agar and by calculating a non-linear regression fit to a semi-log

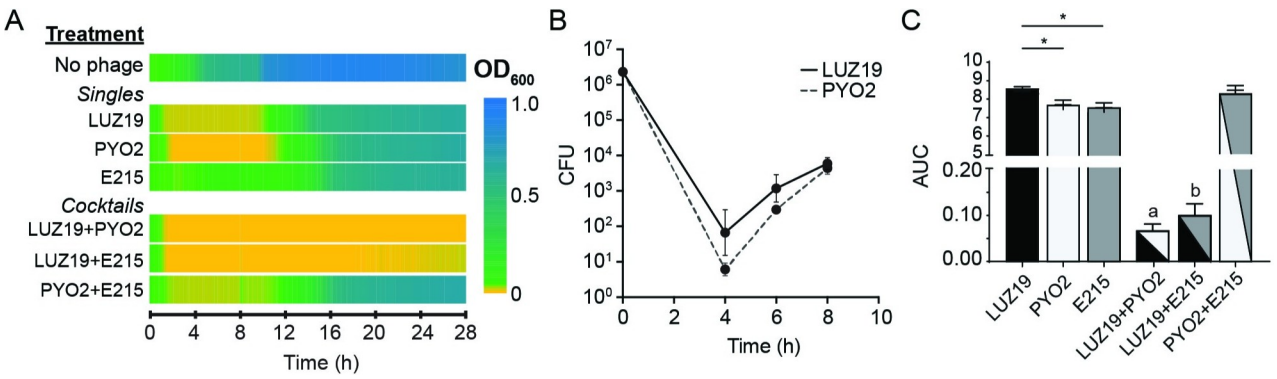

Fig 2. ***In vitro*** **time-kill kinetics. (A)** Heatmap representation of PAO1 treated with single phage strains LUZ19, PYO2, or E215 (MOI 1) and combination strains LUZ19+E215, LUZ19+PYO2, or PYO2+E215 (MOI 0.5 per phage). **(B)** Bacterial colony counts (CFU) post treatment with LUZ19 (solid) or PYO2 (dashed). **(C)** Area under the curve (AUC) estimated the amount of bacterial cell density after 28 h of treatment. Treatments denoted as "a" and "b" were significant to each other and all others. $^{*}p < 0.05$

https://doi.org/10.1371/journal.pcsy.0000015.g002

line equation $Y = 10^{(4.22+9.33X)}$ (n = 72). Bacterial counts on agar also show that PYO2 treatment reduced sensitive cells from 2×10^6 to merely 6 CFU after 4 hours, whereas LUZ19 reduced cells counts to 92 CFU after 4 hours (Fig 2B). Although LUZ19 appeared more potent at reducing cell counts compared to PYO2, bacterial counts showed population regrowth by 6 hours post treatment by either phage. Surprisingly, LUZ19 was less effective at suppressing observed bacterial regrowth compared to the seemingly less potent PYO2 in time-kill curves (Fig 2A). In addition, time-kill area under the curve (AUC) showed that LUZ19 allowed for 15% higher bacterial burden than PYO2 (Fig 2C). Nonetheless, bacterial population rebound implied that cells emerged insensitive to either phage infection. In contrast, E215 showed a marked difference in activity. Despite E215 and PYO2 binding to the same LPS O-antigen, E215 did not reduce the bacterial population but rather caused sustained growth constraint for 14 hours (Fig 2A). This implied the phage lysis rate was less than the expected bacterial exponential growth rate. Consequently, bacterial population regrowth was delayed the longest with the least potent E215 treatment.

Phage cocktails, in comparison to monophage therapy, are typically used to treat individual and/or multi-strain infections since bacteria are less likely to develop resistance when attacked by multiple phages simultaneously [14]. We formulated three different 2-phage cocktails LUZ19+PYO2, LUZ19+E215, and PYO2+E215. We then determined if the bacteriolytic effect of a 2-phage cocktail produced a more efficient reduction in bacterial density compared to the component phage strains. Cocktails however did not appear to increase the rate of bacterial decline in time-kill curves, with declines being similar to the most potent phage in the cocktail. For example, LUZ19+PYO2 and LUZ19+E215 exhibited bacterial reductions comparable to that of LUZ19 alone, dropping the cell density below the LOD within ~3 hours (Fig 2A). As expected, the major benefit of a cocktail was significant improvement in phage resistance suppression, which significantly lowered the time-kill AUC (Fig 2C). Despite most LUZ19+PYO2 and LUZ19+E215 treated cultures appearing visually clear, about 10% showed bacterial regrowth after 26 hours of treatment. Cocktail treatment using LUZ19+PYO2 reduces the bacterial population to the lowest density found in this study (Fig 2A). In contrast, PYO2+E215 showed no significant improvement in bacterial reduction or resistance suppression and AUC was similar to individual treatments with its component phages (Fig 2A and 2C).

Assessment of the survivors

Because *P. aeruginosa* could survive both mono and two-phage treatments, insensitive isolates were whole genome sequenced to verify mutational-based resistance. We found cell surface modifications as the main resistance mechanisms for all three phage strains. Nonsynonymous mutations of type IV pilus genes could block LUZ19 infection and mutations of a lipopolysaccharide O-antigen gene could block both PYO2 and E215 infection (Fig 3A and S1 Table). LUZ19 treatment selected for point mutations in any of several genes encoding type IV pilus machinery, including *pilR* (pilin), *pilB* (assembly), *pilF* (secretin), and *pilZ* (assembly) (S1 Table). In contrast, we found PYO2 and E215 selected for point mutations or deletions in a single gene, *wzy*, which confirmed that these phages bind to the same cell surface receptor. Because chromosomal mutations that, although not exclusively, modify or delete phage cell surface receptors are frequently associated with adaptation [67], we reasoned that surface cell receptor mutations would be the most likely mechanism of phage resistance. Among double-resistant populations that emerged during LUZ19+E215 treatment, 4/5 isolates harbored mutations in both *wzy* and *pil* genes (Fig 3A). We identified only the expected *pil* gene mutation in the fifth isolate despite the bacterial mutant having resistance to both LUZ19 and E215. Similarly, only 1/5 isolates from LUZ19+PYO2 treated cultures had both *wzy* and *pil* gene mutations (Fig 3A). Consistent with expected collateral resistance, 4/5 isolates from PYO2 +E215 treatments had mutations in the *wzy* gene (Fig 3A). Other gene mutations may have also resulted in observed phage resistance, which remain to be determined. It is also worth mentioning that PAO1 populations maintained a majority susceptibility to each phage in the absence of treatment.

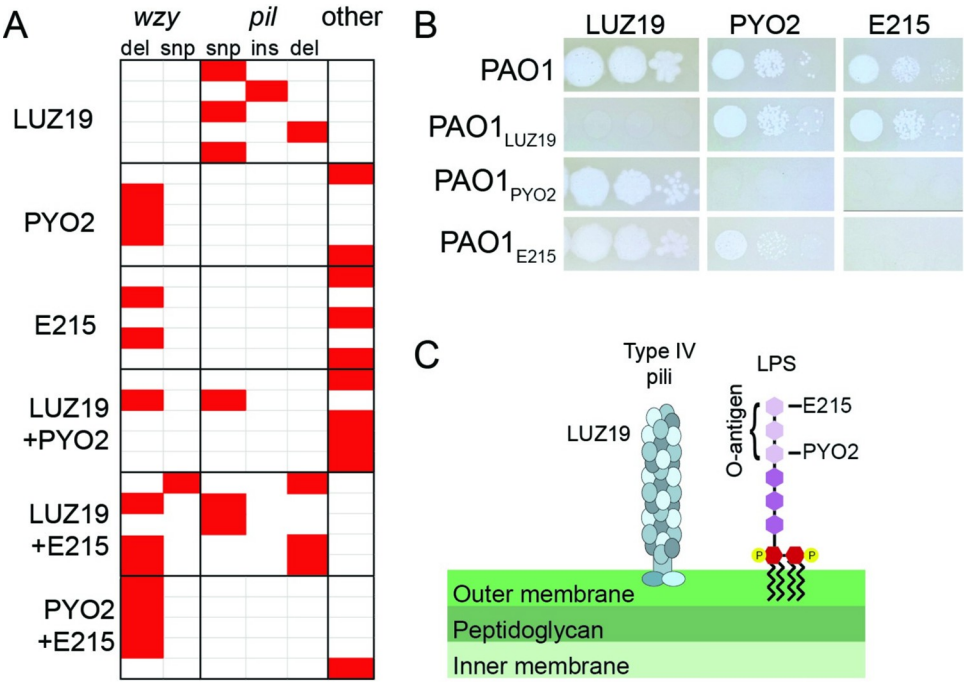

Fig 3. *In vitro* and bioinformatic analyses of phage resistant PAO1 mutants. (A) Heatmap representation of mutations identified using BRESEQ post phage treatment. Phage resistant mutations in genes besides LPS or pili are denoted as "other". **(B)** Efficacy of plating comparison of wild-type PAO1 and phage resistant PAO1 strains. **(C)** Diagram of phage receptor binding mechanisms for each of the three phages. LUZ19 binds to type IV pili while phages PYO2 and E215 both bind to the LPS O-antigen.

https://doi.org/10.1371/journal.pcsy.0000015.g003

Efficacy of plating (EOP) showed that mutations in *pil* genes did not exhibit a reduced sensitivity to the LPS binding phages PYO2 and E215 (Fig 3B). Likewise, mutations in the *wzy* gene did not affect LUZ19 EOP. As to be expected, E215 was unable to infect PYO2-resistant mutants since they share the same cell surface receptor. The inverse however was not always true; PYO2 could infect some E215-resistant mutants, albeit with a lower EOP (Fig 3B). This suggests that E215 and PYO2 bind to different regions of the O-antigen (for proposed binding site schematic, see Fig 3C). The differential phage sensitivity profiles support the ability of specific phage combinations to delay the emergence of phage resistance.

Parameter estimation: *in vitro* growth rate of sensitive bacteria

Individual cultures of *P. aeruginosa* were grown at 37˚C for 28 hours to calibrate a baseline growth rate in the absence of phage infection. We used 89 independent experimental growth curves to generate a logistic model to predict the growth of phage sensitive PAO1. We then calibrated the basal growth rate, r_n, in the logistic growth equation for B, given by:

$$\frac{dB}{dt} = r_n B(1 - \frac{B}{K}) \tag{6}$$

S1 Fig shows the result of this curve fit created using a least-squares fit with FindFit in Wolfram Mathematica; see Table 1 for the estimated growth parameters.

Model parameter estimation: time-kill kinetics of single phage treatment

Combining our *in silico* model with *in vitro* results we were able to examine the changes in bacterial populations below the LOD. Treatment using phages LUZ19 and PYO2 successfully reduced the bacterial burden below LOD within 4 hours (Fig 4A and 4B), while E215 could not in the same timeframe (Fig 4C). We therefore categorize LUZ19 and PYO2 as having greater potency than E215. Moreover, bacterial re-growth was observed between 10–13 hours, suggesting the emergence of a phage resistant population. We estimated parameter values of phage binding *b*, lysis *s*, and mutation *a*, and rates with the system of equations from our single phage interaction model using the BFGS algorithm implemented in Julia's Optim packageusing FindFit. For each phage treatment, we fitted an ensemble of models with different initial conditions to at least 30 independent experimental growth curves, and we obtained the parameter confidence intervals through bootstrapping for around 1000 samples. However, we make the following assumptions about the system for our calibrations:

i. We approximated that the OD_{600} conversion to CFU/mL using the equation $Y = 10^{(4.22 + 9.33X)}$, where X is the OD_{600} value.

ii. All phages undergo strictly lytic replication and binding of phage to bacteria is irreversible and lead to infection. There are differences in the binding mechanism used by each phage. However, the large number of infections occurring dominates the size of the rate term. That is the physical contact of the bacteria and phage should effectively equal each phage's binding rate *b* on a population scale.

iii. Different phage strains have different lysis rates *s*, indicating their different potencies. The average lifespan of an infected cell before lysis is given by *1/s*. The phage specific lysis rates s_a, s_b, and s_c were estimated from the respective in vitro time-kill kinetics. Consistent with the experimental phage latent periods (Table 1 and S2 Fig), the model was able to estimate individual phage lysis rates.

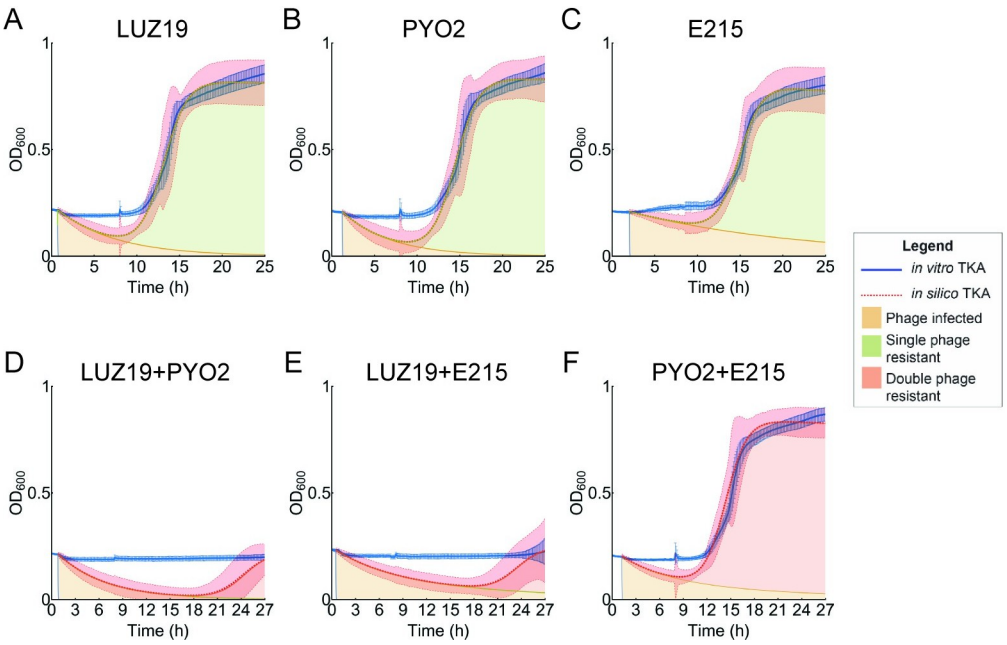

Fig 4. ***In vitro*** **and** ***in silico*** **time-kill kinetics. (A-C)** *In vitro* curves (blue) of phages **(A)** LUZ19, **(B)** PYO2, and **(C)** E215 treatment at MOI 1. Data shown as mean ± standard error of mean (SEM) of replicate wells (n>11). The curves flatten at the limit of detection (LOD) OD_{600} ~0.2. The logistic growth rate of phage infected cells B_I (orange) and resistant cells B_R (green) were fitted according to Eq 1. 95% confidence interval of model fitting is included as shaded area. **(D-F)** *In vitro* growth curve (blue) of cocktails **(D)** LUZ19+PYO2, **(E)** LUZ19+E215, or **(F)** PYO2+E215. Logistic growth rate of phage infected cells B_I (orange), single-mutant resistant cells B_{R1} and B_{R2} (green), and double-mutant resistant cells B_{R12} (red) were fitted according to Eq 4 **(D-E)** and 5 **(F)**.

https://doi.org/10.1371/journal.pcsy.0000015.g004

iv. The mutation rates were estimated from regrowth timing in the time-kill assay (Fig 4). There is no large difference in the per gene mutation rate, denoted in Eq (1), on a molecular level across different strains of bacteria. However, according to mutational analysis there were 7 potential gene mutations that could convey resistance to the pili-binding LUZ19 and only one gene for PYO2 or E215 (S2 Table). Accordingly, our model parameter estimation found that the rate of generating pili-binding phage (e.g. LUZ19) resistance a_p, was 3-fold higher than the rate of generating LPS-binding phage (e.g. PYO2 and E215) resistance a_l (i.e., $a_p > a_l$) (Table 1).

v. The growth rate of single phage resistant bacteria, r_r, was estimated by fitting Eq (6) to *in vitro* fitness assays performed on assumed phage insensitive populations (Fig 1 and S1 Fig). However, the remaining parameters in the model either represent combination actions or were not measurable in isolation from experiments.

Model solution and sensitivity: Single phage treatment

Fig 5 models the simulated population densities of the treatment phages and of phage sensitive, phage infected, and phage resistant bacteria when phages are administered at a MOI of 1. The model predicts kinetics differently for each of the phage strains. In general, the model predicts that the sensitive bacteria decrease after the phage density reaches the inundation threshold (Eq 3) and thereafter the phage population surges (Eq 2). Eventually, the resistant bacterial population dominates the culture. As expected, the more potent phages LUZ19 and PYO2 replicate faster and reduce sensitive cells faster than the relatively less potent phage E215 (Fig 5A–5C). A

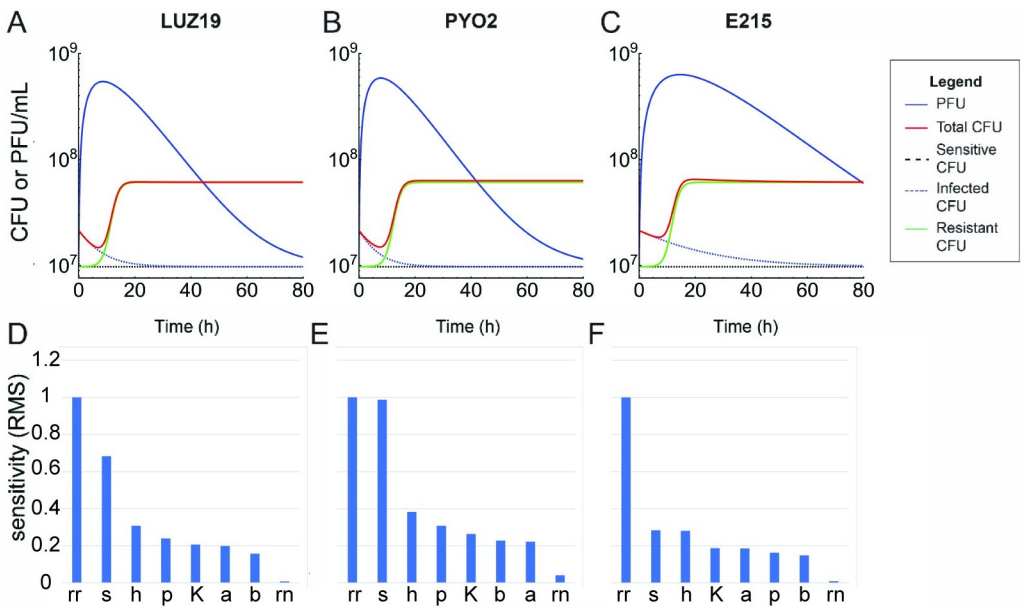

Fig 5. ***In silico*** **single phage modeling and parameter sensitivities.** ***(A-C)*** *Single phage model numerical simulations:* ***(A)*** *LUZ19 only treatment,* ***(B)*** *PYO2 only treatment, and* ***(C)*** *E215 only treatment. For all the simulations,* $B(0) = 0.2$, $B_I(0) = 0$, $B_R(0) = 0$, $P(0) = 0.2$, $b = 382$, *and* $r_n = 0.88$. *For each simulation, phage specific parameter values are in Table 1.* ***(D-F)*** *Sensitivity analysis for the single phage model of each phage parameter settings. The relative sensitivities of* ***(D)*** *LUZ19,* ***(E)*** *PYO2, and* ***(F)*** *E215 were analyzed as outlined in Appendix A.*

https://doi.org/10.1371/journal.pcsy.0000015.g005

drawback of eliminating sensitive cells faster however is that the more potent phages decay in the system sooner. E215 sustained a higher density of phages for roughly twice as long as either of the other two phages (Fig 5C). Additionally, our model simulations (S4 Fig) indicate that the initial MOI does not significantly change the overall dynamics of bacteria and phage. Specifically, for the three phages selected, variations in the initial MOI only slightly impact the timing of bacterial re-growth, likely because these phages replicate rapidly and reach their peak within a few hours. For clinical application, knowing the precise bacterial count in a patient is typically not feasible, making MOI-based analyses less practical. Therefore, for simplicity, we focused mainly on an MOI of 1 in this manuscript.

Because not all parameter values were experimentally determined, we also studied the local and global sensitivity of the calibrated parameters for individual phage's kinetics to determine possible areas of concern. The methods for this analysis are described in S1 Text, S2 Text, Fig 5D–5F, and S3 Fig. Each phage had slightly different sensitivity profiles. The growth rate of the phage sensitive bacteria was the most sensitive parameter. The lytic characteristics (lysis rate s, burst size h) of phage replication were most important for the more potent phages LUZ19 and PYO2. In contrast, E215 was less sensitive to these parameters. By detailing the dependence of the model outcome on phage specific lysis properties, it is interesting to note that PYO2 and E215 showed higher sensitivity to burst size h, resistant bacterial growth r_r, and binding rate b, while LUZ19 showed sensitivity to bacterial growth r_n. Again, the mechanism of infection for phage LUZ19 differs from that of phage PYO2 and E215 and appears to influence overall system activity.

Leveraging the mathematical model to prevent phage resistance with single phage therapy

Next, we sought to leverage our mathematical model to identify the phage infection characteristics with the highest therapeutic potential. Because the model defines lysis rate and burst size

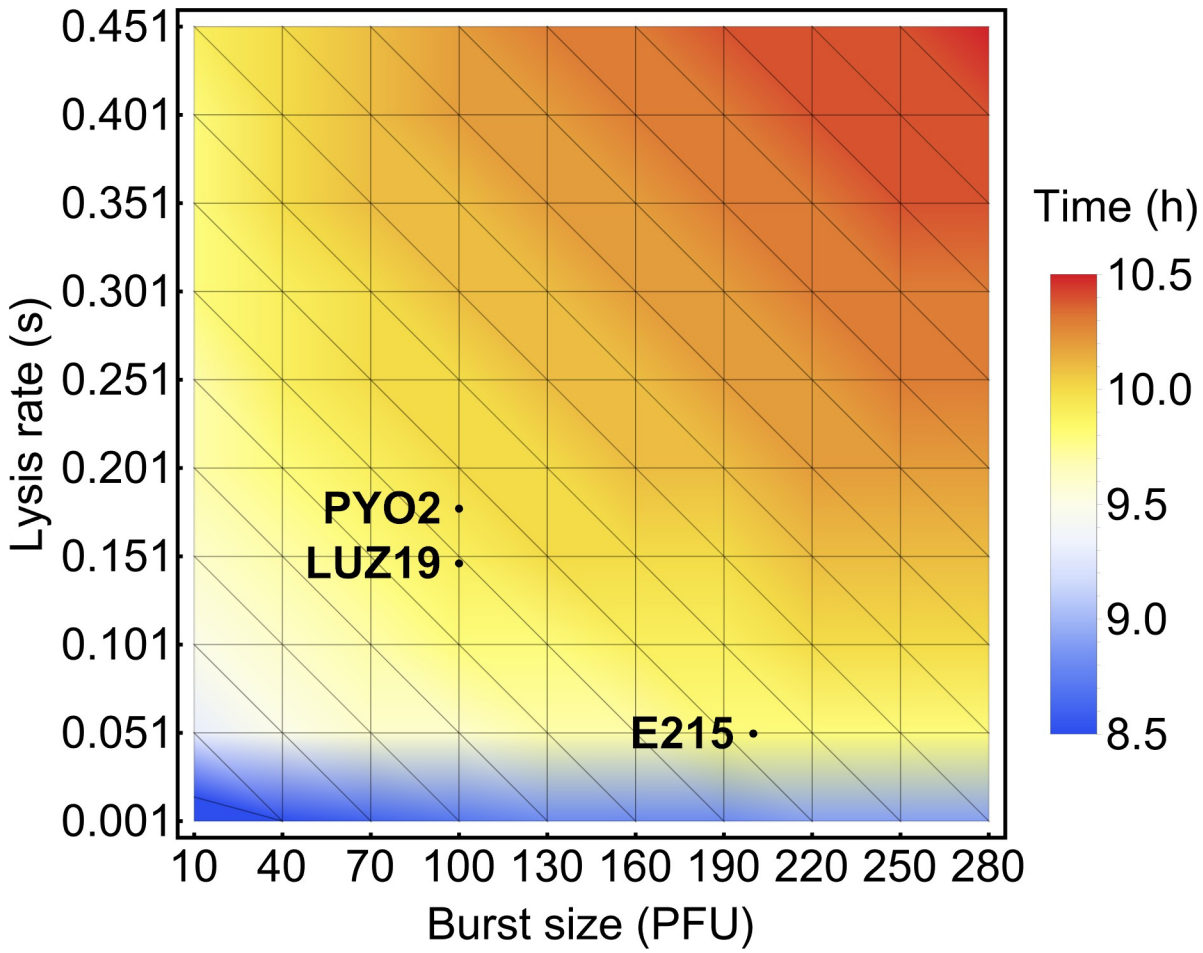

Fig 6. *In silico* determination of optimal phage infection characteristics. Different combinations of phage lysis rate (*s*) and burst size (*h*) and their corresponding time for the resistant bacteria to become detectable. The marked points denote our experimental phage strains.

https://doi.org/10.1371/journal.pcsy.0000015.g006

dependent on phage strain, we simulated the characteristic combinations with the most potential in preventing the emergence of phage resistance. For each parameter combination, we simulate the single phage model and find the times with which resistant bacterial density exceeds the time-kill curve LOD (Fig 6). We found that the model predicts that a phage with both a large burst size and high lysis rate would delay the occurrence of resistance more effectively. Model predictions agreed with experimentally determined phage latent periods and burst size correlations with time kill curves (S2 Fig). In addition, when the lysis rate is low, the time of resistance occurrence is more sensitive to the change in lysis rate relative to the burst size. When the lysis rate is large enough, the time of resistance occurrence becomes more sensitive to the change in burst size relative to the lysis rate. PYO2 and LUZ19 are more effective at delaying the occurrence of phage resistance due to their high potency, or lysis rate. However, despite E215 having a burst size twice that of PYO2 and LUZ19, its slower lysis rate limits its ability to delay the occurrence of resistance.

Model parameter estimation: time-kill kinetics of two-phage treatment

Next, we extended our single-phage model to describe phage–phage combination kinetics with the assumption that phage resistance does not confer collateral resistance to the other

phage strain (For model schematic see Fig 1B). It is generally accepted that phage cocktails can better inhibit the evolution of resistance and thereby increased the longevity of the treatment [14,64,65,68]. That is, the probability of two different resistance mutations occurring in a single host cell can be significantly lower than that of only acquiring a single mutation depending on the phage receptors and pairing [66]. We also explored whether combining phage strains enhance treatment potency compared to single phage therapy. Our two-phage treatment models (Eqs 4 and 5) are used, in part, to simulate the interactions between phage and bacteria in an *in vitro* setting in order to study the effectiveness of different cocktail formulations. That is, Eq 4 simulated when phage LUZ19 was applied with an LPS-binding phage (PYO2 or E215), while Eq 5 simulated when the two LPS-binding phages were combined. Basal growth rates of "double-mutants" (mutations in both the *pil* and *wzy* genes), r_{a+b} for LUZ19+PYO2 treatment, and r_{a+c}, for cocktail LUZ19+E215 treatment were calibrated from phage resistant bacterial growth with Eq 6 (Fig 4E–4F and S1 Fig).

Calibrated two-phage models were able to incorporate parameters from the single phage model to accurately predict the bacterial kinetics during cocktail treatments (Fig 4D–4F). Simulations agreed with *in vitro* data that combining two potent phages (LUZ19 and PYO2) was more effective at reducing bacterial burden than combining a potent and weak phage (LUZ19 and E215). Consistent with *in vitro* observations, combined action of LUZ19+PYO2 was simulated to reduce the bacterial burden to the lowest level observed using a two-phage cocktail (Fig 1A, Fig 4D). Moreover, double-mutant resistance was not modeled to exceed the LOD during the 28 hour simulation. Comparatively, LUZ19+E215 treatment reduced the bacterial burden below the LOD, but the double-mutant outgrowth begins to emerge as early as ~20 hours after phage treatment (Fig 4E). As expected, the model predicts combing two LPS binding phages (PYO2 and E215) is only as effective as the more potent phage's (PYO2) individual treatment (Fig 4B versus Fig 4F).

Model solution: Time-kill kinetics of two-phage treatment

Fig 7 shows the simulated population densities of cocktail treatment phages and of phage sensitive, phage infected, single-mutant, and double-mutant bacteria when phages are treated at a MOI of 1. The model predicts kinetics differently for treatments depending on the receptors of the phages used, that is, with and without collateral resistance. Consistent with *in vitro*

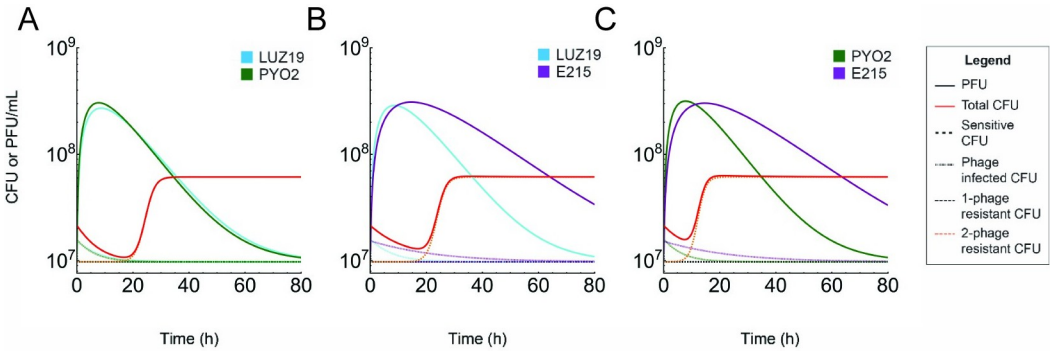

Fig 7. Double phage model numerical simulations. (A-C) Double-phage simulations at MOI 0.5 per phage for: **(A)** LUZ19+PYO2, **(B)** LUZ19+E215, and **(C)** PYO2+E215. Phage concentrations are denoted with solid lines with LUZ19 (blue), PYO2 (green), and E215 (purple). For all the simulations, the black dashed line denotes the sensitive bacteria and the red solid line denotes total bacteria. Infected bacterial strains and single-phage resistant mutants are denoted by tall dashed lines and wide dashed lines respectively in colors corresponding to the target phages. The double-phage double-mutant strain is denoted with an orange dashed line.

https://doi.org/10.1371/journal.pcsy.0000015.g007

findings, the two-phage model predicts that the sensitive bacteria decreases after the phage density reaches the inundation threshold and phage populations increase at the expense of sensitive cells before a resistant bacterial population dominates (Fig 7). Differences arise in the specific combinations. During LUZ19+PYO2 treatment, both phages exhibit nearly symmetrical growth and decay patterns, phages rapidly increase within the first 18 hours of treatment but begin declining shortly thereafter. Following robust phage expansion, resistance is delayed for about 25 hours until the rise of double-mutant cells around 25 hours (Fig 7A). With LUZ19+E215 treatment, phages replicate asymmetrically, the more potent LUZ19 population grows faster compared to E215, which expands more slowly but sustained for nearly 40 hours. Although the E215 population appears to persist throughout the simulation, resistance was only delayed for about 25 hours, shorter than LUZ19+PYO2 despite the persistence of phages (Fig 7B). Although, PYO2 and E215 share the same cell surface receptor, the faster lysis rate of PYO2 allows it to outgrow E215 (Fig 7C). Similar to the LUZ19+E215 cocktail, E215 is still expected to persist for far longer than PYO2 despite their shared receptor mechanism. Ultimately, this treatment also resulted in bacterial growth transients similar to those from PYO2 only treatment, with resistance outgrowth emerging at ~12.5 hours.

Next, because populations of sensitive and resistant bacteria appeared to wax and wane in simulation, we sought to determine if there was an *in vitro* growth tradeoff to having resistance to both a pili binding and LPS binding phage (Fig 8). We performed growth assays and analyzed their growth rates to examine the fitness cost of acquired genotypic resistance (Fig 1, Fig 8 and S1 Fig). Single gene mutations were predicted to cause a slight decrease in mutant growth rate relative to the sensitive bacteria. LUZ19 resistance appears to have a slightly higher fitness cost compared to resistance to an LPS binding phage. Mutants with two mutations arising from cocktail treatments bear significantly higher tradeoff, with LUZ19 and PYO2/E215 resistance having the greatest reduction in relative growth rate (Fig 1, Fig 8, and S1 Fig). Again, although mutations to PYO2 and E215 single treatments resulted in similar genotypic resistance outcomes (S2 Table), the differential binding of the two phages to the O-antigen appears to influence the fitness of the emerged double-mutants to cocktail but not individual treatment (Fig 3C).

Effect of decreased binding rate with different phage treatments

Because the effects of changing the phage adsorption rate may generate additional competition between different bacterial variants, we also simulate hypothetical phage combinations to compare the competitive dynamics between two phages with differential growth characteristics that target a single bacteria host. In the two scenarios we modeled, phages under decreased binding rates (b) competed for susceptible host cells. In the first case phages with inverse properties (low lysis rate and high burst size versus high lysis rate and low burst size) were both able to reproduce high phage densities but were less effective at suppressing the bacterial population (Fig 9A). The phage with higher potency was able to replicate more quickly, reaching its maximum density within 30 hours of addition. On the other hand, the phage with lower potency but higher burst was able to reach a higher population density than its partner, albeit several hours slower and only after the first phage population began decaying. The overall bacterial population on the other hand, was barely reduced by combination phage action and remained high throughout the simulation. Although the phages were able to reduce the initial sensitive cell population, single-mutants resistant to each phage began growing after 10 hours. The population of these phage resistant mutants were inversely correlated to phage population growth and decay. However, the double-mutant population resistant to both phages appeared to outgrow phage activity around 35 hours (Fig 9A). Although a decreased binding rate

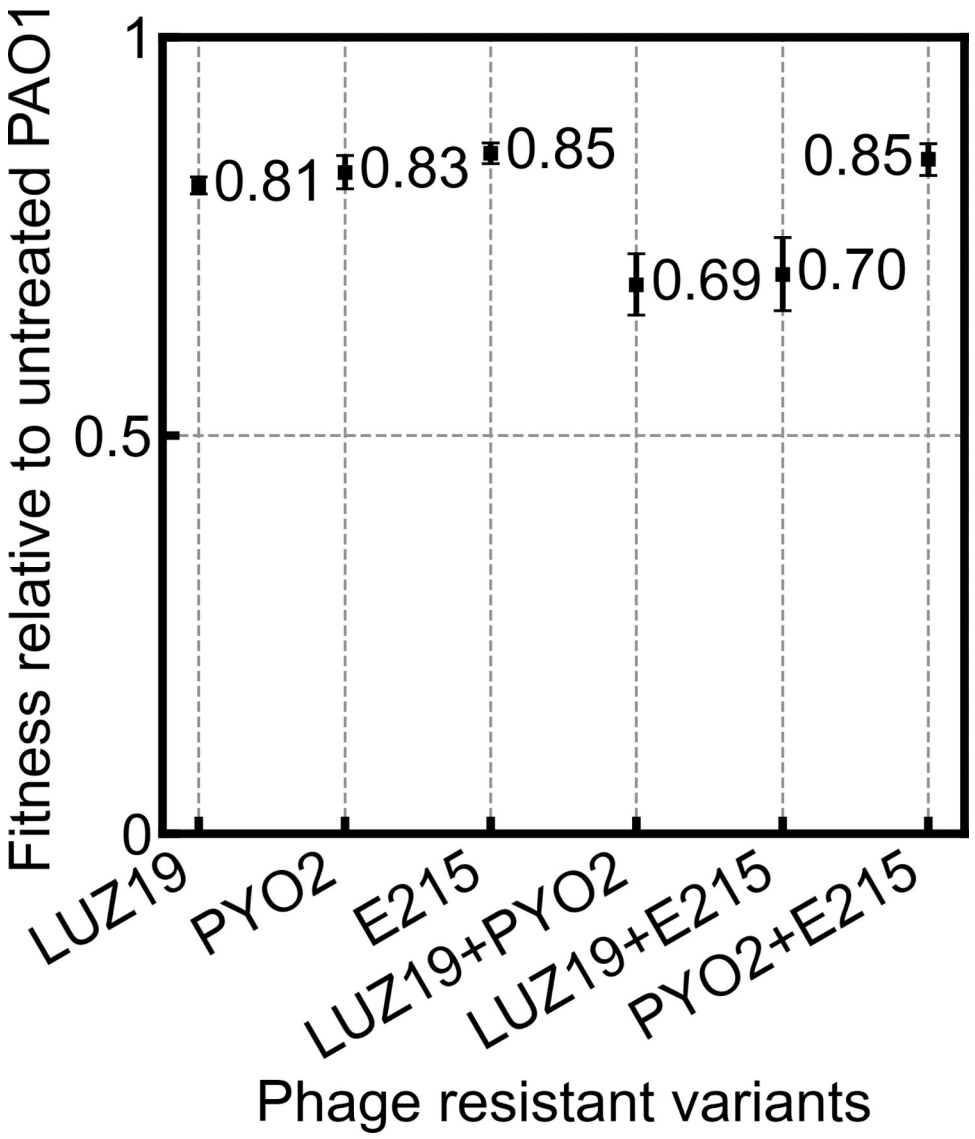

Fig 8. Per capita growth rate of phage resistant variants. Relative growth rates (with 95% confidence intervals) of PAO1 resistant to different single and double phage treatments. Fitness was determined relative to phage sensitive untreated PAO1.

https://doi.org/10.1371/journal.pcsy.0000015.g008

reduces the ability of phage to proliferate and kill susceptible bacteria, it promotes competition between different bacterial strains and thereby delays the occurrence of double-phage resistant bacteria. In the second scenario, phages with opposing characteristics (high lysis and burst versus low lysis and burst) were simulated in combination and demonstrated dynamics more extreme than those we observed from our *in vitro* model (Fig 9B). In this simulation we saw that the high potency, large burst size phage was able to quickly replicate to its maximum density shortly after addition while the alternate phage was almost fully unable to replicate. Single-mutants to the second phage therefore scarcely grew, which suggests that the population of single-mutants to the high potency phage were able to grow rapidly. Of note however, is that the double-mutant resistant to both phages appears unable to grow as quickly in the presence of the abundant single-mutant to the first phage strain. This suggests that when phages have such

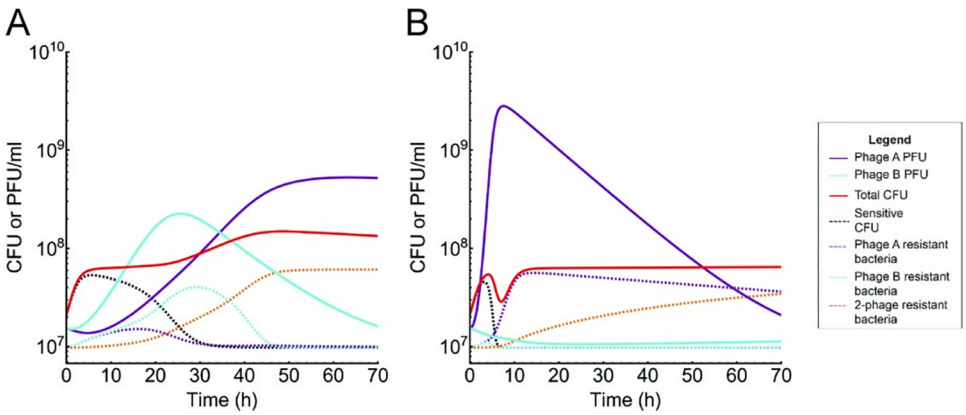

Fig 9. ***In silico*** **cocktail simulations using hypothetical phages.** *Comparison of two-phage cocktail treatments under decreased phage binding rate* b. ***(A)*** *Cocktail treatment of* P_a+P_b *where phage* P_a *has a low lysis rate (s) and high burst size* (h) *and* P_b *inversely has a high lysis rate (potency) and low burst size.* ***(B)*** *Cocktail treatment of* P_a+P_b *where phage* P_a *has both high potency and burst size while* P_b *inversely has low potency and burst size.*

https://doi.org/10.1371/journal.pcsy.0000015.g009

polar characteristics that the potential for alternate cocktail treatment modalities, such as sequential treatment, may potentially extend the longevity of the treatment phages.

Predicting sequential phage therapy outcomes

Phage combinations are frequently given in simultaneous regimens. Alternatively, sequential treatment regimens that temporally or spatially separate the phage strains may offer advantages to individual phage activities, such as our observations when two phages have polar characteristics (Fig 9B). A limitation to performing *in vitro* characterization of different phage-bacteria combinations, however, is the variety of ways in which the system can be administered. For instance, phage order, dose, and timing are all variables that impact the efficacy of treatment. Previously, Wright et al. suggested that sequential phage treatments may cause significantly higher fitness cost compared to multiple phages administered simultaneously as traditionally done with cocktails [14]. Therefore, we simulated sequential two-phage treatments with the second phage added at 8 hours, the estimated time when single phage resistant mutant density would be sufficient to support replication of the second added phage (Fig 10). When simulating sequential treatment, we also reduced the basal growth rates of the double-mutant strains that emerge in the treatment of LUZ19→PYO2 and LUZ19 → E215, denoted as $r_{a\to b}$ and $r_{a\to c}$ respectively, by 10% relative to r_{a+b} and r_{a+c}. This was in contrast to the double-mutant strains that emerge in the treatment of phage PYO2→LUZ19 and E215→LUZ19 which are assumed to have the same growth rate as the double-mutant strains in the corresponding simultaneous cocktail treatments [14]. To ensure that we were relating comparable growth dynamics, we chose a carrying capacity above the max growth reported at 15 hours ($K = 0.9$). The sequential parameters are listed in Table 2; noting that the calibration and assumptions are dependent on the specific phage strain. Sequential treatments were first simulated utilizing the two-phage model without collateral resistance as shown in Eq 4. As in our observations during cocktail treatment, addition of LUZ19 in combination with an LPS binding phage produced the greatest simulated reduction in bacterial density. Addition of LUZ19→PYO2 and PYO2→LUZ19 caused a significant reduction in bacterial density, with the LUZ19→PYO2 regimen being more potent and delaying the growth of double-mutants for longer (Fig 10A–10B). These trends also occur between LUZ19→E215 and E215→LUZ19 sequential treatments (Fig 10C–10D). These predicted outcomes emphasize the importance of

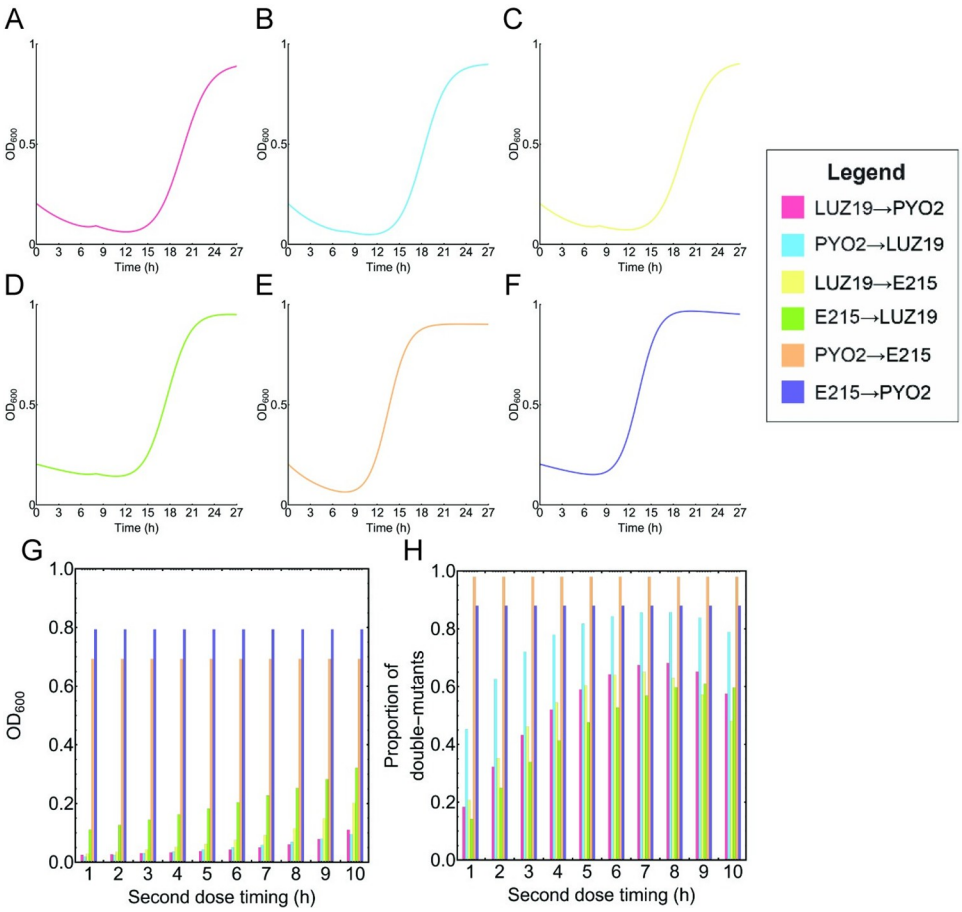

Fig 10. ***In silico*** **experiments for two-phage sequential treatments.** Each curve simulates the total bacteria density (solid line) after adding one phage strain at MOI 1 at time 0, and a different phage strain at MOI 1 at time 8 hours. **(A)** LUZ19→PYO2 (pink); **(B)** PYO2→LUZ19 (blue); **(C)** LUZ19→E215 (yellow); **(D)** E215 →LUZ19 (green); **(E)** PYO2→E215 (orange); **(F)** E215→PYO2 (purple). **(G-H)** Comparison of double phage sequential treatments with different phage combinations, application order, and second dose timings. **(G)** The total bacterial density at 15 hours was used to measure the treatment's ability to control the bacterial population density. **(H)** The proportion of the bacteria at 15 hours that are resistant to all treatment phages.

https://doi.org/10.1371/journal.pcsy.0000015.g010

phage order in addition to phage strain selection. Simulating sequential treatment with two LPS binding phages, we refer to the two-phage mathematical model with collateral resistance (Eq 5). As expected, sequential PYO2→E215 and E215→PYO2 outcomes were consistent with trends observed with simultaneous administration (Fig 10E–10F). Taken together, our simulations imply that all sequential treatments were less effective at controlling bacteria burden than their two-phage simultaneous treatment counterparts despite the assumed fitness cost.

Because we observed different replication kinetics during competition between phages with different characteristics (Fig 9), we rationalized that second dose timing could also affect phage-bacteria kinetics and thus treatment outcomes. Therefore, we extended the sequential model to explore the effect of second phage administration timing. Comparison between different administration times, in one-hour intervals, showed that prolonging the second phage administration correlated with decreases in treatment efficacy (Fig 10G and 10H). As expected, phages that select for collateral resistance were insensitive to a change in second phage timing. Interestingly, prolonging sequential administration initially correlates with a decreased ability

to prevent resistance before improving it. That is, prolonging the second administration past 9 hours was found to elongate the growth period of emerged mutants to the first phage, which competitively suppresses growth of double mutants. Among sequential treatment, administration of E215→LUZ19 could be the most effective in delaying resistance and yet this was not the optimal approach to control bacterial density. LUZ19→PYO2 and LUZ19→E215 were relatively effective at both delaying resistance and efficient at controlling bacterial density. Combined, simultaneous cocktail addition remains the best treatment modality to take advantage of the multiplicative nature of double-mutant phage resistance, but adjusting phage order and sequential timing can improve the kinetics of resistance outcomes.

4 Discussion

In this study, we demonstrated experimentally and mathematically that the simultaneous administration of select phage strains as a cocktail was more effective at controlling *P. aeruginosa* density than phages applied sequentially or individually. By combining *in vitro* and *in silico* models of time-kill kinetics, we show 74 permutations of single, double simultaneous, or double sequential phage treatments. Of these, we found that double simultaneous treatment with LUZ19+PYO2 was the most potent at reducing bacterial density. The increased potency also promoted a more robust phage growth of both LUZ19 and PYO2 over a longer period. In contrast, double simultaneous treatment with different cocktails of LUZ19+E215 or PYO2 +E215 exhibited weaker potency. In addition, double sequential treatments initially lack compounding phage infectivities and were subsequently lower in potency. Sequential treatment potency could be increased comparable to double simultaneous LUZ19 and PYO2 treatment by reducing the interval between administrations to less than two hours. As to be expected, we show that combining phages that bind to different cell surface receptors suppressed bacterial numbers far longer than combining phages that bind to the same receptor. Nevertheless, evolution of resistance could not be prevented with a cocktail composed of phages that bind to different cell surface receptors. Resistance did impose fitness costs on emerged mutants by hampering their growth by as much as 31%. Together, a formulation with two highly potent phage strains and those that bind asymmetrically were determined to be essential cofactors for superior treatment efficacy of a phage cocktail.

Lytic activity is a critically important attribute to phage therapy. Of the three phages, PYO2 was the most potent at reducing bacterial numbers whereas E215 was unable to reduce bacteria, rather it could only restrain bacterial growth when administered at the same MOI. Stronger potency was achieved when PYO2 and LUZ19 were combined, leading to further reduction in bacterial density by up to 15%. On the other hand, combining two phages that exhibit a high potency and a low potency provided no greater bacterial suppression than the most potent phage strain in that cocktail. Phage replication is divided into the phases of virion attachment, DNA entry, replication, virion assembly and finally, egress via cell lysis. It is not clear how PYO2 was the most potent at reducing *P. aeruginosa*, nor why combining multiple phages lead to a higher potency of a cocktail. These findings suggest that certain phages have a genetic constitution better suited for exploiting host cell surface receptors, intracellular resources, DNA-synthesis, and protein-synthesis systems, and/or degrading structural components [69,70]. For other phage strains, the opposite may be true. Therefore, treatment potency is an indication of not only the quantity required to produce a lytic effect, but also the lysis efficiency of the phage agents. The complexity of each phage strain implies that determining individual phage potency is required for adequate cocktail development.

Moreover, treatments employing two potent phage strains that have asymmetrical cell surface receptors was the strongest predictor of therapy 'longevity'. Double simultaneous LUZ19

and PYO2 treatment provided the longest suppression of the *P. aeruginosa* population as compared to other treatment scenarios. Cocktail treatment eventually failed due to resistance development to both phage strains. By combining phages with asymmetrical receptors, the joint probability of two or more resistance mutations occurring in a single bacterial cell would be governed by the multiplication rule of probabilities [71]. Although two nonsynonymous mutations within a single cell occurred during cocktail treatment, the emergence of a double mutant was significantly delayed due to a lower probability of both mutations occurring. That is, the probability of occurrence of both receptor *pil* and *wzy* gene mutations is equal to the product of the probability of *wzy* gene mutation occurring and the conditional probability that event *pil* mutation occurring given that *wzy* gene mutation occurs. This implies that phages in a cocktail can 'synergize' to extend treatment longevity by multiplying their resistance probabilities. Next, we investigated whether administering phages sequentially was viable as an alternative strategy to extend the replication of phages and suppress the evolution of phage resistance rather than only delaying resistance [72,73]. Our mathematical model predicts that double sequential phage therapy would not be as effective as double simultaneous therapy at preventing resistance. We theorize that sequential treatment does not fully exploit the multiplication rule of probabilities across the bacterial population [71]. Sequential treatment allows a host cell to rapidly acquire a mutation to escape the first phage and these resistant mutants would grow unabated until the addition of the second phage strain. The secondary phage would then encounter two bacterial subpopulations, one sensitive to both phage strains and the other sensitive to only the second phage. The latter subpopulation would not experience a multiplication rule of probabilities and thus the probability of gaining a resistance mutation would be similar to administering a single phage alone. Therefore, we predict that the appearance of mutants resistant to both phage strains would occur sooner than if the phages were treated simultaneously.

Phage resistance remains a major challenge for phage therapy [74,75]. The fate of evolved resistance mutants however is determined in part by their fitness to compete with non-mutant counterparts and maintain its virulence [76]. We found *in vitro* and *in silico* that single receptor gene mutations did not impose significant fitness trade-offs in growth rate under prevailing conditions in the absence of phage. However, evolved mutants with two receptor gene mutations (e.g., *pil* and *wzy*) experienced a higher cost of resistance, seen by a decline in growth rate of up to 31% in the absence of phages compared to cells. These findings agreed with previous reports that single-receptor mutations may be of little consequence to the bacterial cell, whereas multiple mutations elicit an unavoidable cost [14,64]. Wright et al. similarly showed that the growth rate of evolved independent resistance to two phage strains was significantly decreased [14]. Markwitz et al. further identified other fitness costs to evolved resistance to multiple *P. aeruginosa* phage strains including motility, virulence, and sensitivity to human serum [64]. This implies that evolved multi-phage resistant cells can outcompete non-mutant sensitive bacteria in the presence of phages, but resistant variants would be at a growth disadvantage in the absence of phages. In the body, this may occur between phage cocktail administrations due to the rapid decay of phages [18,77].

Phages are unlike other antimicrobials in that they self-dose (i.e., replicate) during treatment. When PYO2 and LUZ19 are administered together, our mathematical model predicts that both phages would grow evenly to a similar maximum density. In contrast, administering either PYO2 and E215 or LUZ19 and E215 together, the phages grow unevenly. E215 is predicted to replicate not as well nor reach as high of a concentration when paired with either PYO2 or LUZ19. Since a bacterial cell can only be infected by a single phage, increasing phage strain diversity also introduces the possibility for phage competition [73]. As mentioned, host competitive ability varied among the three phages tested. The reduction in productivity that

E215 may experience in the presence of competitors provides evidence that multiple infections can have a severe impact on self-dosing. Because host competitive ability was independent of pairing phages that use the same cell surface receptor (PYO2 and E215), phage compete in replication efficiency. E215 replication cycle takes longer than the other phages and thus, there is a lag of new progeny to infect susceptible cells. Susceptible cells are monopolized by the more efficiently replicating phages, further perpetuating E215 growth demise as its progeny have fewer new cells to infect. This competitive exclusion suggests two phages cannot coexist when infecting the same host bacterium. Betts et al. similarly found that pairwise phages in double simultaneous treatments experienced less viral growth in the absence of phage competition [73]. We found further evidence of this when simulating sequential treatments. Our mathematical model predicts that higher total phage growth occurred during double simultaneous treatment compared to double sequential treatment. This is because all susceptible cells initially supported single phage replication instead of supporting replication of two phages. By the time the second phage strain is administered, the susceptible population numbers are low and unable to support robust amplification of the second phage. In addition, both phages are now competing for the small population of susceptible cells. This would suggest that simultaneous treatment provides greater productivity of each phage component to maximize self-dosing. The genetic and physiological factors that determine the outcome of host competition appear to be of critical importance to cocktail design, yet they remain poorly understood.

Mathematical tools are instrumental to understanding complex biological systems. Models help us parameterize, control, and optimize our predictions while allowing us to study the effects of changing each component and/or treatment condition in the system. In this study, we developed multiple mathematical models that incorporated both phage synergy and the stepwise evolution of the bacteria to multiple phages to provide a mechanistic description of the kinetics between the bacteria and two phage strains. This was an extension of the models developed by Payne & Jansen and Cairns [28,31,43]. We have introduced two versions of the double phage treatment model, with and without collateral resistance. Thus, when novel phages with known receptors are introduced, our models can use individual phage killing and evolutionary parameters to infer the treatment's efficacy. We calibrated our models and used them as plug-and-play frameworks to explore more treatment regimens and scenarios, such as the sequential treatments with different dosing intervals, solutions with decreased phage binding rate, and of selecting from hypothetical phage choices. By adopting a simplified approach within a well-mixed experimental environment, we uncovered subtle details of bacteria-phage interactions and drew general conclusions about key phage characteristics.

However, our model has limitations. Future work could investigate the best methods to capture the emergence of phage-resistant bacteria, potentially requiring stochastic modeling to replicate observed phenomena [78,79]. Additionally, exploring more realistic heterogeneous mixing could reduce reliance on the homogeneous mixing assumption for phage infection rates. In particular, some studies found that phage are less efficient at dealing with well-established biofilms compared to well-mixed systems, since the spatial heterogeneity of biofilms hinders phage propagation and biofilm clearance [80,81]. Hence, incorporating spatial structure into future *in vivo* models may be crucial for the effective application of phage therapy in clinical settings. Moreover, in clinical settings, patients often receive both phage therapy and antibiotics [82]. Phage-resistant bacteria may remain susceptible to antibiotics, making a combined treatment of phage cocktail therapy and antibiotics effective. Evidence suggests that while phages do not trigger an immune response, bacteria-boosted innate immunity activity can act against the phages [27]. This finding may explain instances of phage ineffectiveness and suggests that better protocols for phage therapy could be developed. Therefore, a long-term goal is to build a biologically realistic *in vivo* model of treatment therapy that explores the

effects of multiple phage strains on the bacterial population including spatial structure, in conjunction with antibiotics and immune response dynamics. This comprehensive approach will lead to the optimal design of phage therapy treatments.

5 Conclusions

In conclusion, we found that the optimal pairwise phage treatment strategy was the double simultaneous administration of two highly potent and asymmetrically binding phage strains. This treatment regimen had the greatest lysis efficiency, reduced bacterial density the most, and suppressed the evolution of resistance for the longest duration. However, this cocktail treatment strategy could not prevent phage resistance *in vitro*. Further study of three-phage cocktails, with three unique binding receptors, may limit resistance since the multiplication of two mutation probabilities only led to delayed resistance. We found that double sequential phage treatment had several drawbacks compared to double simultaneous administration. However, a sequential regimen may have other benefits not explored in this study, such as limiting the emergence of neutralizing anti-phage immune responses [12,83]. Together, these results highlight that the pharmacokinetics and pharmacodynamics of each phage are important in designing a therapeutic cocktail. Future work to map which phage properties enhance potency is necessary to optimize multi-phage cocktail treatment regimens.

Supporting information

S1 Table. Genotypic and phenotypic characteristics of phage strains.
(DOCX)

S2 Table. Identity, function, position, and types of mutations identified *in vitro*.
(DOCX)

S1 Fig. (A) Growth of *P. aeruginosa* PAO1 without the addition of phage (blue curve) and a logistic curve fit. **(B-G)** Growth curves of PAO1 resistant to LUZ19, PYO2, E215, LUZ19 +E215, LUZ19+PYO2, and PYO2+E215 over 18 hours. Data (blue shaded area) shown as mean ± standard error of mean (SEM) of replicate wells ($n>11$). 95% confidence interval of model fitting is included as an orange shaded area.
(DOCX)

S2 Fig. PYO2 (black) and E215 (blue) growth characteristics during incubation at 37˚C with shaking. **(A)** Adsorption rates (K, $phage^{-1}$ $cell^{-1}$ mL^{-1} min^{-1}) were determined by measuring the decline of free-phage in a phage-bacteria solution at a MOI of 0.02. Measurements were taken every minute for 12 min. Adsorption rates ($K_{adsorption}$) were calculated when 50% of free-phage remained in solution. **(B)** One-step growth curves were performed to determine the eclipse, latent period, and burst size per cell of phage infection. Phages were mixed with bacteria at a MOI of 0.1 and samples were taken every 2 min until the plateau of free-phage. Samples were divided to calculate the eclipse period (derived from CHCl3 treatment), latent period (derived from untreated samples), and burst size (calculated from the average plateau point between untreated and CHCl3 treatment divided by the difference in titer at t = 7 of untreated and treated samples).
(DOCX)

S3 Fig. Partial Rank Correlation Coefficient (PRCC) for Total Bacteria in the single phage model. Significant p-values ($p<0.01$) indicated with *.
(DOCX)

S4 Fig. Single phage model (Eq 1) simulation using the same parameter values as Fig 5A–5C but with different initial MOIs. (A-C) Model solutions for three different MOIs of LUZ19 treated at time 0; (D-F) Model solutions for three different MOIs of PYO2 treated at time 0; (G-I) Model solutions for three different MOIs of E215 treated at time 0.
(DOCX)

S1 Text. Local sensitivity analysis.
(DOCX)

S2 Text. Global sensitivity analysis.
(DOCX)

Acknowledgments

This research group was initially formed during the Collaborative Workshop for Women in Mathematical Biology hosted by the Institute for Pure and Applied Mathematics at the University of California, Los Angeles in June 2019. The authors would like to thank Dr. Aadrita Nandi and Allison Hedin for their discussion. The authors would also like to acknowledge the contribution of the late Dr. Mary Ann Horn. The authors would also like to thank the handling editor and reviewers for their helpful comments and suggestions, which improved the presentation of the manuscript.

Author Contributions

Conceptualization: Zhiyuan Yu, Tiffany Luong, Selenne Banuelos, Hwayeon Ryu, Rebecca Segal, Dwayne R. Roach, Qimin Huang.

Data curation: Zhiyuan Yu, Tiffany Luong, Dwayne R. Roach.

Formal analysis: Zhiyuan Yu, Selenne Banuelos, Hwayeon Ryu, Rebecca Segal, Qimin Huang.

Funding acquisition: Hwayeon Ryu, Rebecca Segal, Dwayne R. Roach, Qimin Huang.

Investigation: Tiffany Luong, Andrew Sue, Dwayne R. Roach.

Methodology: Zhiyuan Yu, Selenne Banuelos, Rebecca Segal, Dwayne R. Roach, Qimin Huang.

Project administration: Rebecca Segal, Dwayne R. Roach.

Resources: Dwayne R. Roach.

Software: Zhiyuan Yu, Rebecca Segal, Qimin Huang.

Supervision: Dwayne R. Roach, Qimin Huang.

Validation: Qimin Huang.

Visualization: Zhiyuan Yu, Tiffany Luong, Selenne Banuelos, Rebecca Segal, Dwayne R. Roach, Qimin Huang.

Writing – original draft: Zhiyuan Yu, Tiffany Luong, Selenne Banuelos, Qimin Huang.

Writing – review & editing: Zhiyuan Yu, Tiffany Luong, Selenne Banuelos, Hwayeon Ryu, Rebecca Segal, Dwayne R. Roach, Qimin Huang.

References

1. Luong T, Salabarria AC, Roach DR. Phage therapy in the resistance era: where do we stand and where are we going? Clin Ther. 2020; 42(9):1659–80. Epub 2020/09/05. https://doi.org/10.1016/j.clinthera.2020.07.014 PMID: 32883528.
2. Petrovic Fabijan A, Iredell J, Danis-Wlodarczyk K, Kebriaei R, Abedon ST. Translating phage therapy into the clinic: recent accomplishments but continuing challenges. PLoS Biol. 2023; 21(5):e3002119. Epub 2023/05/23. https://doi.org/10.1371/journal.pbio.3002119 PMID: 37220114; PubMed Central PMCID: PMC10204993.
3. Adams MH. Bacteriophages. Bacteriophages. 1959.
4. Hendrix RW, Smith MC, Burns RN, Ford ME, Hatfull GF. Evolutionary relationships among diverse bacteriophages and prophages: all the world's a phage. Proc Natl Acad Sci U S A. 1999; 96(5):2192–7. Epub 1999/03/03. https://doi.org/10.1073/pnas.96.5.2192 PMID: 10051617; PubMed Central PMCID: PMC26759.
5. Breitbart M, Rohwer F. Here a virus, there a virus, everywhere the same virus? Trends in microbiology. 2005; 13(6):278–84. https://doi.org/10.1016/j.tim.2005.04.003 PMID: 15936660
6. Suh GA, Lodise TP, Tamma PD, Knisely JM, Alexander J, Aslam S, et al. Considerations for the use of phage therapy in clinical practice. Antimicrob Agents Chemother. 2022; 66(3):e0207121. Epub 2022/01/19. https://doi.org/10.1128/AAC.02071-21 PMID: 35041506; PubMed Central PMCID: PMC8923208.
7. Law N, Logan C, Yung G, Furr CL, Lehman SM, Morales S, et al. Successful adjunctive use of bacteriophage therapy for treatment of multidrug-resistant Pseudomonas aeruginosa infection in a cystic fibrosis patient. Infection. 2019; 47(4):665–8. Epub 2019/05/19. https://doi.org/10.1007/s15010-019-01319-0 PMID: 31102236.
8. Van Nieuwenhuyse B, Van der Linden D, Chatzis O, Lood C, Wagemans J, Lavigne R, et al. Bacteriophage-antibiotic combination therapy against extensively drug-resistant *Pseudomonas aeruginosa* infection to allow liver transplantation in a toddler. Nat Commun. 2022; 13(1):5725. Epub 2022/09/30. https://doi.org/10.1038/s41467-022-33294-w PMID: 36175406; PubMed Central PMCID: PMC9523064.
9. Dedrick RM, Smith BE, Cristinziano M, Freeman KG, Jacobs-Sera D, Belessis Y, et al. Phage therapy of *Mycobacterium* infections: compassionate use of phages in 20 patients with drug-resistant Mycobacterial disease. Clin Infect Dis. 2023; 76(1):103–12. Epub 2022/06/10. https://doi.org/10.1093/cid/ciac453 PMID: 35676823; PubMed Central PMCID: PMC9825826.
10. Chan BK, Stanley G, Modak M, Koff JL, Turner PE. Bacteriophage therapy for infections in CF. Pediatr Pulmonol. 2021; 56 Suppl 1:S4–S9. Epub 2021/01/13. https://doi.org/10.1002/ppul.25190 PMID: 33434411.
11. Danis-Wlodarczyk K, Dabrowska K, Abedon ST. Phage therapy: the pharmacology of antibacterial viruses. Curr Issues Mol Biol. 2021; 40(1):81–164. Epub 2020/06/07. https://doi.org/10.21775/cimb.040.081 PMID: 32503951.
12. Champagne-Jorgensen K, Luong T, Darby T, Roach DR. Immunogenicity of bacteriophages. Trends in Microbiology. 2023; 31(10):1058–71. https://doi.org/10.1016/j.tim.2023.04.008 PMID: 37198061
13. Fernandez L, Rodriguez A, Garcia P. Phage or foe: an insight into the impact of viral predation on microbial communities. ISME J. 2018; 12(5):1171–9. Epub 2018/01/27. https://doi.org/10.1038/s41396-018-0049-5 PMID: 29371652; PubMed Central PMCID: PMC5932045.
14. Wright RCT, Friman VP, Smith MCM, Brockhurst MA. Resistance evolution against phage combinations depends on the timing and order of exposure. mBio. 2019; 10(5):10.1128/mbio. 01652–19. Epub 2019/09/26. https://doi.org/10.1128/mBio.01652-19 PMID: 31551330; PubMed Central PMCID: PMC6759759.
15. Brockhurst MA, Koskella B, Zhang Q-G. Bacteria-phage antagonistic coevolution and the implications for phage therapy. Bacteriophages: biology, technology, therapy. 2021:231–51.
16. Wendling CC, Lange J, Liesegang H, Sieber M, Pohlein A, Bunk B, et al. Higher phage virulence accelerates the evolution of host resistance. Proc Biol Sci. 2022; 289(1984):20221070. Epub 2022/10/06. https://doi.org/10.1098/rspb.2022.1070 PMID: 36196537; PubMed Central PMCID: PMC9532999.
17. Blazanin M, Turner PE. Community context matters for bacteria-phage ecology and evolution. ISME J. 2021; 15(11):3119–28. Epub 2021/06/16. https://doi.org/10.1038/s41396-021-01012-x PMID: 34127803; PubMed Central PMCID: PMC8528888 Inc.
18. Roach DR, Leung CY, Henry M, Morello E, Singh D, Di Santo JP, et al. Synergy between the host immune system and bacteriophage is essential for successful phage therapy against an acute respiratory pathogen. Cell Host Microbe. 2017; 22(1):38–47 e4. Epub 2017/07/14. https://doi.org/10.1016/j.chom.2017.06.018 PMID: 28704651.

19. Rodriguez-Gonzalez RA, Leung CY, Chan BK, Turner PE, Weitz JS. Quantitative models of phage-antibiotic combination therapy. Msystems. 2020; 5(1):e00756–19. Epub 2020/02/06. https://doi.org/10.1128/mSystems.00756-19 PMID: 32019835; PubMed Central PMCID: PMC7002117.

20. Li G, Leung CY, Wardi Y, Debarbieux L, Weitz JS. Optimizing the timing and composition of therapeutic phage cocktails: a control-theoretic approach. Bull Math Biol. 2020; 82(6):75. Epub 2020/06/14. https://doi.org/10.1007/s11538-020-00751-w PMID: 32533350; PubMed Central PMCID: PMC8272981.

21. Leung CYJ, Weitz JS. Modeling the synergistic elimination of bacteria by phage and the innate immune system. J Theor Biol. 2017; 429:241–52. Epub 2017/07/03. https://doi.org/10.1016/j.jtbi.2017.06.037 PMID: 28668337.

22. Banuelos S, Gulbudak H, Horn MA, Huang Q, Nandi A, Ryu H, et al. Investigating the impact of combination phage and antibiotic therapy: a modeling study. Using Mathematics to Understand Biological Complexity: From Cells to Populations. 2021:111–34.

23. Smith NM, Nguyen TD, Chin WH, Sanborn JT, de Souza H, Ho BM, et al. A mechanism-based pathway toward administering highly active N-phage cocktails. Front Microbiol. 2023; 14:1292618. Epub 2023/12/04. https://doi.org/10.3389/fmicb.2023.1292618 PMID: 38045026; PubMed Central PMCID: PMC10690594.

24. Delattre R, Seurat J, Haddad F, Nguyen TT, Gaborieau B, Kane R, et al. Combination of *in vivo* phage therapy data with *in silico* model highlights key parameters for pneumonia treatment efficacy. Cell Rep. 2022; 39(7):110825. Epub 2022/05/19. https://doi.org/10.1016/j.celrep.2022.110825 PMID: 35584666.

25. Jeon J, Park JH, Yong D. Efficacy of bacteriophage treatment against carbapenem-resistant *Acinetobacter baumannii* in *Galleria mellonella* larvae and a mouse model of acute pneumonia. BMC Microbiol. 2019; 19(1):70. Epub 2019/04/04. https://doi.org/10.1186/s12866-019-1443-5 PMID: 30940074; PubMed Central PMCID: PMC6444642.

26. Uchiyama J, Rashel M, Takemura I, Wakiguchi H, Matsuzaki S. *In silico* and *in vivo* evaluation of bacteriophage phiEF24C, a candidate for treatment of *Enterococcus faecalis* infections. Appl Environ Microbiol. 2008; 74(13):4149–63. Epub 2008/05/06. https://doi.org/10.1128/AEM.02371-07 PMID: 18456848; PubMed Central PMCID: PMC2446516.

27. Hodyra-Stefaniak K, Miernikiewicz P, Drapala J, Drab M, Jonczyk-Matysiak E, Lecion D, et al. Mammalian host-versus-phage immune response determines phage fate *in vivo*. Sci Rep. 2015; 5(1):14802. Epub 2015/10/07. https://doi.org/10.1038/srep14802 PMID: 26440922; PubMed Central PMCID: PMC4594097.

28. Cairns BJ, Timms AR, Jansen VA, Connerton IF, Payne RJ. Quantitative models of *in vitro* bacteriophage-host dynamics and their application to phage therapy. PLoS Pathog. 2009; 5(1):e1000253. Epub 2009/01/03. https://doi.org/10.1371/journal.ppat.1000253 PMID: 19119417; PubMed Central PMCID: PMC2603284.

29. Berryhill BA, Huseby DL, McCall IC, Hughes D, Levin BR. Evaluating the potential efficacy and limitations of a phage for joint antibiotic and phage therapy of *Staphylococcus aureus* infections. Proc Natl Acad Sci U S A. 2021; 118(10):e2008007118. Epub 2021/03/03. https://doi.org/10.1073/pnas.2008007118 PMID: 33649203; PubMed Central PMCID: PMC7958385.

30. Schmerer M, Molineux IJ, Bull JJ. Synergy as a rationale for phage therapy using phage cocktails. PeerJ. 2014; 2:e590. Epub 2014/10/04. https://doi.org/10.7717/peerj.590 PMID: 25279269; PubMed Central PMCID: PMC4179555.

31. Payne RJ, Jansen VA. Understanding bacteriophage therapy as a density-dependent kinetic process. J Theor Biol. 2001; 208(1):37–48. Epub 2001/02/13. https://doi.org/10.1006/jtbi.2000.2198 PMID: 11162051.

32. Hesse E, Best A, Boots M, Hall A, Buckling A. Spatial heterogeneity lowers rather than increases host–parasite specialization. Journal of evolutionary biology. 2015; 28(9):1682–90. https://doi.org/10.1111/jeb.12689 PMID: 26135011

33. Korobeinikov A, Shchepakina E, Sobolev V. The paradox of enrichment, spatial heterogeneity, community effects and the phenomenon of apparent disappearance in the marine bacteriophage dynamics. The ANZIAM Journal. 2020; 62(4):453–68.

34. Forti F, Roach DR, Cafora M, Pasini ME, Horner DS, Fiscarelli EV, et al. Design of a broad-range bacteriophage cocktail that reduces *Pseudomonas aeruginosa* biofilms and treats acute infections in two animal models. Antimicrob Agents Chemother. 2018; 62(6):10.1128/aac.02573-17. Epub 2018/03/21. https://doi.org/10.1128/AAC.02573-17 PMID: 29555626; PubMed Central PMCID: PMC5971607.

35. Henry M, Lavigne R, Debarbieux L. Predicting *in vivo* efficacy of therapeutic bacteriophages used to treat pulmonary infections. Antimicrob Agents Chemother. 2013; 57(12):5961–8. Epub 2013/09/18. https://doi.org/10.1128/AAC.01596-13 PMID: 24041900; PubMed Central PMCID: PMC3837875.

36. Debarbieux L, Leduc D, Maura D, Morello E, Criscuolo A, Grossi O, et al. Bacteriophages can treat and prevent *Pseudomonas aeruginosa* lung infections. J Infect Dis. 2010; 201(7):1096–104. Epub 2010/03/04. https://doi.org/10.1086/651135 PMID: 20196657.

37. Cafora M, Forti F, Briani F, Ghisotti D, Pistocchi A. Phage therapy application to counteract *Pseudomonas aeruginosa* infection in cystic fibrosis zebrafish embryos. J Vis Exp. 2020;(159). Epub 2020/06/02. https://doi.org/10.3791/61275 PMID: 32478753.

38. Forti F, Bertoli C, Cafora M, Gilardi S, Pistocchi A, Briani F. Identification and impact on *Pseudomonas aeruginosa* virulence of mutations conferring resistance to a phage cocktail for phage therapy. Microbiol Spectr. 2023:e0147723. Epub 2023/11/15. https://doi.org/10.1128/spectrum.01477-23 PMID: 37966242.

39. Uyttebroek S, Chen B, Onsea J, Ruythooren F, Debaveye Y, Devolder D, et al. Safety and efficacy of phage therapy in difficult-to-treat infections: a systematic review. Lancet Infect Dis. 2022; 22(8):e208–e20. Epub 2022/03/07. https://doi.org/10.1016/S1473-3099(21)00612-5 PMID: 35248167.

40. Lin DM, Koskella B, Lin HC. Phage therapy: an alternative to antibiotics in the age of multi-drug resistance. World J Gastrointest Pharmacol Ther. 2017; 8(3):162–73. Epub 2017/08/23. https://doi.org/10.4292/wjgpt.v8.i3.162 PMID: 28828194; PubMed Central PMCID: PMC5547374.

41. Campbell A. Conditions for the existence of bacteriophage. Evolution. 1961; 15(2):153–65. https://doi.org/10.2307/2406076

42. Levin BR, Stewart FM, Chao L. Resource-limited growth, competition, and predation: a model and experimental studies with bacteria and bacteriophage. The American Naturalist. 1977; 111(977):3–24.

43. Payne RJ, Phil D, Jansen VA. Phage therapy: the peculiar kinetics of self-replicating pharmaceuticals. Clin Pharmacol Ther. 2000; 68(3):225–30. Epub 2000/10/03. https://doi.org/10.1067/mcp.2000.109520 PMID: 11014403.

44. Weitz JS, Hartman H, Levin SA. Coevolutionary arms races between bacteria and bacteriophage. Proc Natl Acad Sci U S A. 2005; 102(27):9535–40. Epub 2005/06/25. https://doi.org/10.1073/pnas.0504062102 PMID: 15976021; PubMed Central PMCID: PMC1172273.

45. Bull JJ, Levin BR, Molineux IJ. Promises and pitfalls of *in vivo* evolution to improve phage therapy. Viruses. 2019; 11(12):1083. Epub 2019/11/27. https://doi.org/10.3390/v11121083 PMID: 31766537; PubMed Central PMCID: PMC6950294.

46. Weld RJ, Butts C, Heinemann JA. Models of phage growth and their applicability to phage therapy. J Theor Biol. 2004; 227(1):1–11. Epub 2004/02/19. https://doi.org/10.1016/S0022-5193(03)00262-5 PMID: 14969703.

47. Styles KM, Brown AT, Sagona AP. A review of using mathematical modeling to improve our understanding of bacteriophage, bacteria, and eukaryotic interactions. Front Microbiol. 2021; 12:724767. Epub 2021/10/09. https://doi.org/10.3389/fmicb.2021.724767 PMID: 34621252; PubMed Central PMCID: PMC8490754.

48. Lavigne R, Lecoutere E, Wagemans J, Cenens W, Aertsen A, Schoofs L, et al. A multifaceted study of *Pseudomonas aeruginosa* shutdown by virulent podovirus LUZ19. mBio. 2013; 4(2):e00061–13. Epub 2013/03/21. https://doi.org/10.1128/mBio.00061-13 PMID: 23512961; PubMed Central PMCID: PMC3604761.

49. Brandao A, Pires DP, Coppens L, Voet M, Lavigne R, Azeredo J. Differential transcription profiling of the phage LUZ19 infection process in different growth media. RNA Biol. 2021; 18(11):1778–90. Epub 2021/01/16. https://doi.org/10.1080/15476286.2020.1870844 PMID: 33448239; PubMed Central PMCID: PMC8583145.

50. Ceyssens PJ, Glonti T, Kropinski NM, Lavigne R, Chanishvili N, Kulakov L, et al. Phenotypic and genotypic variations within a single bacteriophage species. Virol J. 2011; 8:134. Epub 2011/03/25. https://doi.org/10.1186/1743-422X-8-134 PMID: 21429206; PubMed Central PMCID: PMC3072928.

51. Li F, Hou CD, Lokareddy RK, Yang R, Forti F, Briani F, et al. High-resolution cryo-EM structure of the *Pseudomonas* bacteriophage E217. Nat Commun. 2023; 14(1):4052. Epub 2023/07/09. https://doi.org/10.1038/s41467-023-39756-z PMID: 37422479; PubMed Central PMCID: PMC10329688.

52. Luong T, Salabarria AC, Edwards RA, Roach DR. Standardized bacteriophage purification for personalized phage therapy. Nat Protoc. 2020; 15(9):2867–90. Epub 2020/07/28. https://doi.org/10.1038/s41596-020-0346-0 PMID: 32709990.

53. Kropinski AM. Measurement of the rate of attachment of bacteriophage to cells. Methods Mol Biol. 2009; 501:151–5. Epub 2008/12/11. https://doi.org/10.1007/978-1-60327-164-6_15 PMID: 19066819.

54. Chevallereau A, Blasdel BG, De Smet J, Monot M, Zimmermann M, Kogadeeva M, et al. Next-generation "-omics" approaches reveal a massive alteration of host RNA metabolism during bacteriophage infection of *Pseudomonas aeruginosa*. PLoS Genet. 2016; 12(7):e1006134. Epub 2016/07/06. https://doi.org/10.1371/journal.pgen.1006134 PMID: 27380413; PubMed Central PMCID: PMC4933390.

55. Chen S, Zhou Y, Chen Y, Gu J. fastp: an ultra-fast all-in-one FASTQ preprocessor. Bioinformatics. 2018; 34(17):i884–i90. Epub 2018/11/14. https://doi.org/10.1093/bioinformatics/bty560 PMID: 30423086; PubMed Central PMCID: PMC6129281.

56. Bankevich A, Nurk S, Antipov D, Gurevich AA, Dvorkin M, Kulikov AS, et al. SPAdes: a new genome assembly algorithm and its applications to single-cell sequencing. J Comput Biol. 2012; 19(5):455–77. Epub 2012/04/18. https://doi.org/10.1089/cmb.2012.0021 PMID: 22506599; PubMed Central PMCID: PMC3342519.

57. Bosi E, Donati B, Galardini M, Brunetti S, Sagot MF, Lio P, et al. MeDuSa: a multi-draft based scaffolder. Bioinformatics. 2015; 31(15):2443–51. Epub 2015/03/27. https://doi.org/10.1093/bioinformatics/btv171 PMID: 25810435.

58. Aziz RK, Bartels D, Best AA, DeJongh M, Disz T, Edwards RA, et al. The RAST Server: rapid annotations using subsystems technology. BMC Genomics. 2008; 9:75. Epub 2008/02/12. https://doi.org/10.1186/1471-2164-9-75 PMID: 18261238; PubMed Central PMCID: PMC2265698.

59. Deatherage DE, Barrick JE. Identification of mutations in laboratory-evolved microbes from next-generation sequencing data using breseq. Methods Mol Biol. 2014; 1151:165–88. Epub 2014/05/20. https://doi.org/10.1007/978-1-4939-0554-6_12 PMID: 24838886; PubMed Central PMCID: PMC4239701.

60. Bertozzi Silva J, Storms Z, Sauvageau D. Host receptors for bacteriophage adsorption. FEMS Microbiol Lett. 2016; 363(4). Epub 2016/01/13. https://doi.org/10.1093/femsle/fnw002 PMID: 26755501.

61. Klann M, Koeppl H. Spatial simulations in systems biology: from molecules to cells. Int J Mol Sci. 2012; 13(6):7798–827. Epub 2012/07/28. https://doi.org/10.3390/ijms13067798 PMID: 22837728; PubMed Central PMCID: PMC3397560.

62. Bull JJ, Christensen KA, Scott C, Jack BR, Crandall CJ, Krone SM. Phage-bacterial dynamics with spatial structure: self organization around phage sinks can promote increased cell densities. Antibiotics. 2018; 7(1):8. https://doi.org/10.3390/antibiotics7010008 PMID: 29382134

63. Heldal M, Bratbak G. Production and decay of viruses in aquatic environments. Marine Ecology Progress Series. 1991; 72(3):205–12.

64. Markwitz P, Olszak T, Gula G, Kowalska M, Arabski M, Drulis-Kawa Z. Emerging phage resistance in *Pseudomonas aeruginosa* PAO1 Is accompanied by an enhanced heterogeneity and reduced virulence. Viruses. 2021; 13(7). Epub 2021/08/11. https://doi.org/10.3390/v13071332 PMID: 34372538; PubMed Central PMCID: PMC8310095.

65. Oechslin F. Resistance development to bacteriophages occurring during bacteriophage therapy. Viruses. 2018; 10(7). Epub 2018/07/04. https://doi.org/10.3390/v10070351 PMID: 29966329; PubMed Central PMCID: PMC6070868.

66. Dettman JR, Sztepanacz JL, Kassen R. The properties of spontaneous mutations in the opportunistic pathogen *Pseudomonas aeruginosa*. BMC Genomics. 2016; 17:27. Epub 2016/01/07. https://doi.org/10.1186/s12864-015-2244-3 PMID: 26732503; PubMed Central PMCID: PMC4702332.

67. Labrie SJ, Samson JE, Moineau S. Bacteriophage resistance mechanisms. Nat Rev Microbiol. 2010; 8(5):317–27. Epub 2010/03/30. https://doi.org/10.1038/nrmicro2315 PMID: 20348932.

68. Merabishvili M, Pirnay JP, De Vos D. Guidelines to compose an ideal bacteriophage cocktail. Methods Mol Biol. 2018; 1693:99–110. Epub 2017/11/10. https://doi.org/10.1007/978-1-4939-7395-8_9 PMID: 29119435.

69. Weinbauer MG. Ecology of prokaryotic viruses. FEMS Microbiol Rev. 2004; 28(2):127–81. Epub 2004/04/28. https://doi.org/10.1016/j.femsre.2003.08.001 PMID: 15109783.

70. Rampersad S, Tennant P. Replication and expression strategies of viruses. In: Tennant P, Fermin G, Foster JE, editors. Viruses: Academic Press; 2018. p. 55–82.

71. Kleinman A. The mathematics of random mutation and natural selection for multiple simultaneous selection pressures and the evolution of antimicrobial drug resistance. Stat Med. 2016; 35(29):5391–400. Epub 2016/08/09. https://doi.org/10.1002/sim.7070 PMID: 27501057; PubMed Central PMCID: PMC6175190.

72. Hall AR, De Vos D, Friman VP, Pirnay JP, Buckling A. Effects of sequential and simultaneous applications of bacteriophages on populations of *Pseudomonas aeruginosa in vitro* and in wax moth larvae. Appl Environ Microbiol. 2012; 78(16):5646–52. Epub 2012/06/05. https://doi.org/10.1128/AEM.00757-12 PMID: 22660719; PubMed Central PMCID: PMC3406105.

73. Betts A, Gifford DR, MacLean RC, King KC. Parasite diversity drives rapid host dynamics and evolution of resistance in a bacteria-phage system. Evolution. 2016; 70(5):969–78. Epub 2016/03/24. https://doi.org/10.1111/evo.12909 PMID: 27005577; PubMed Central PMCID: PMC4982092.

74. Suh GA, Patel R. Clinical phage microbiology: a narrative summary. Clin Microbiol Infect. 2023; 29(6):710–3. Epub 2023/02/23. https://doi.org/10.1016/j.cmi.2023.02.006 PMID: 36805835.

75. Oromi-Bosch A, Antani JD, Turner PE. Developing phage therapy that overcomes the evolution of bacterial resistance. Annu Rev Virol. 2023; 10(1):503–24. Epub 2023/06/03. https://doi.org/10.1146/annurev-virology-012423-110530 PMID: 37268007.

76. Mangalea MR, Duerkop BA. Fitness trade-offs resulting from bacteriophage resistance potentiate synergistic antibacterial strategies. Infect Immun. 2020; 88(7). Epub 2020/02/26. https://doi.org/10.1128/IAI.00926-19 PMID: 32094257; PubMed Central PMCID: PMC7309606.

77. Tiwari BR, Kim S, Rahman M, Kim J. Antibacterial efficacy of lytic *Pseudomonas* bacteriophage in normal and neutropenic mice models. J Microbiol. 2011; 49(6):994–9. Epub 2011/12/29. https://doi.org/10.1007/s12275-011-1512-4 PMID: 22203564.

78. Vidurupola SW, Allen LJS. Impact of Variability in Stochastic Models of Bacteria-Phage Dynamics Applicable to Phage Therapy. Stoch Anal Appl. 2014; 32(3):427–49. https://doi.org/10.1080/07362994.2014.889922 WOS:000334994000004.

79. Chae D. Phage-host-immune system dynamics in bacteriophage therapy: basic principles and mathematical models. Transl Clin Pharmacol. 2023; 31(4):167–90. Epub 20231122. https://doi.org/10.12793/tcp.2023.31.e17 PMID: 38196997; PubMed Central PMCID: PMC10772058.

80. Testa S, Berger S, Piccardi P, Oechslin F, Resch G, Mitri S. Spatial structure affects phage efficacy in infecting dual-strain biofilms of. Commun Biol. 2019; 2. ARTN 405. WOS:000493963200002.

81. Simmons EL, Bond MC, Koskella B, Drescher K, Bucci V, Nadell CD. Biofilm Structure Promotes Coexistence of Phage-Resistant and Phage-Susceptible Bacteria. Msystems. 2020; 5(3). https://doi.org/10.1128/mSystems.00877-19 WOS:000576704400015. PMID: 32576653

82. Chibani-Chennoufi S, Sidoti J, Bruttin A, Kutter E, Sarker S, Brussow H. In vitro and in vivo bacteriolytic activities of *Escherichia coli* phages: implications for phage therapy. Antimicrob Agents Chemother. 2004; 48(7):2558–69. https://doi.org/10.1128/AAC.48.7.2558-2569.2004 PMID: 15215109; PubMed Central PMCID: PMC434175.

83. Dedrick RM, Freeman KG, Nguyen JA, Bahadirli-Talbott A, Smith BE, Wu AE, et al. Potent antibody-mediated neutralization limits bacteriophage treatment of a pulmonary *Mycobacterium abscessus* infection. Nat Med. 2021; 27(8):1357–61. Epub 2021/07/10. https://doi.org/10.1038/s41591-021-01403-9 PMID: 34239133; PubMed Central PMCID: PMC8571776.